Dalton Transactions

Kinetics and mechanisms of catalytic water oxidation

Journal:	*Dalton Transactions*
Manuscript ID	DT-PER-10-2018-004341.R1
Article Type:	Perspective
Date Submitted by the Author:	29-Nov-2018
Complete List of Authors:	Fukuzumi, Shunichi; Graduate School of Engineering, Osaka University, Department of Material and Life Science Lee, Yong-Min; Ewha Womans University, Department of Chemistry and Nano Science Nam, Wonwoo; Ewha Womans University, Chemistry

Dalton Transactions

CRITICAL REVIEW

Kinetics and mechanisms of catalytic water oxidation

Shunichi Fukuzumi,*[ab] Yong-Min Lee*[ac] and Wonwoo Nam*[ad]

Received 00th October 2018,
Accepted 00th 0000 2018

DOI: 10.1039/x0xx00000x

www.rsc.org/

Kinetics and mechanisms of thermal and photochemical oxidation of water with homogeneous and heterogeneous catalysts, including conversion from homogeneous to heterogeneous catalysts in the course of water oxidation, are discussed in this review article. Molecular and homogeneous catalysts have advantage to clarify the catalytic mechanisms by detecting active intermediates in the catalytic water oxidation. On the other hand, heterogeneous nanoparticle catalysts have advantages for practical applications due to the high catalytic activity, robustness and easier separation of catalysts by filtration as compared with the molecular homogeneous precursors. Ligand oxidation of homogeneous catalysts sometimes results in dissociation of ligands to form nanoparticles, which act as much more efficient catalysts for water oxidation. Since it is quite difficult to identify active intermediates on the heterogeneous catalyst surface, the mechanism of water oxidation has hardly been clarified under heterogeneous catalytic conditions. This review focuses on kinetics and mechanisms of catalytic water oxidation with homogeneous catalysts, which may be converted to heterogeneous nanoparticle catalysts depending on various reaction conditions.

1. Introduction

Clean and sustainable energy production using solar energy has become more and more important as the world energy demand increases due to population growth and global industrialisation.[1-7] Extensive efforts have been made to produce solar fuels as an artificial version of photosynthesis.[7-26] Artificial photosynthesis is composed of light harvesting and charge-separation processes together with catalytic processes for the oxidation of water to evolve O_2 and the reduction of water to evolve H_2, which can be combined with CO_2 fixation. Photoinduced energy transfer and charge-separation (CS) processes in the photosynthetic reaction centres in Photosystem I (PSI) and Photosystem II (PSII) have been well mimicked and many model compounds were synthesized to study the photodynamics extensively.[27-50] With regard to hydrogen evolution reaction (HER), various metal nanoparticles (MNPs) have been used as efficient HER catalysts.[51-73] Homogeneous catalysts have also been developed for CO_2 fixation by H_2 under normal pressure of H_2 and CO_2 at ambient temperature.[74-83] The most difficult part to be further developed in the artificial version of natural photosynthesis is the catalytic water oxidation reaction (WOR) to release four electrons and four protons to evolve O_2. In natural photosynthesis, the water oxidation catalyst (WOC) consists of a manganese-oxo-calcium cluster (Mn_4CaO_5) in the oxygen evolving complex (OEC) in PSII.[84-93]

Both molecular (homogeneous) and solid-state (heterogeneous) catalysts have been employed for chemical, electrocatalytic and photocatalytic oxidation of water.[94-121] In the case of homogeneous WOC, reactive intermediates such as high-valent metal-oxo species are detected during the WOR and the kinetic analysis of the catalytic WOR provides new insights into the rate-determining step (r.d.s.) as well as the catalytic mechanism.[94-108,122-131] However, there is a critical issue to be clarified; that is whether metal complexes supported by organic ligands act as molecular and homogeneous catalysts or precursors of nanoparticle catalysts formed in the course of the WOR acting as much more reactive heterogeneous WOC.[132,133] In order to identify true WOCs, much caution should be exercised to analyse time profiles, kinetic order and to detect reactive intermediates for homogeneous metal complexes when those could be converted to more active metal oxide NPs in the course of the WORs. Thus, this review focuses on kinetics and mechanisms of WORs with homogeneous catalysts including the conversion of molecular homogeneous catalysts to metal oxide or hydroxide NPs that act as truly active heterogeneous catalysts in the oxygen evolution reaction (OER), providing insights into development of much more efficient and robust WOCs.

[a] Department of Chemistry and Nano Science, Ewha Womans University, Seoul 03760, Korea. Email: fukuzumi@chem.eng.osaka-u.ac.jp, yomlee@ewha.ac.kr, wwnam@ewha.ac.kr.
[b] Graduate School of Science and Engineering, Meijo University, Nagoya, Aichi 468-8502, Japan.
[c] Research Institute for Basic Sciences, Ewha Womans University, Seoul 03760, Korea.
[d] State Key Laboratory for Oxo Synthesis and Selective Oxidation, Suzhou Research Institute of LICP, Lanzhou Institute of Chemical Physics (LICP), Chinese Academy of Sciences, Lanzhou 730000, China.

Shunichi Fukuzumi obtained Bachelor, Master and PhD degrees in chemical engineering and applied chemistry at Tokyo Institute of Technology in 1973, 1975 and 1978, respectively. After working as a postdoctoral fellow at Indiana University in USA from 1978 to 1981, he became an Assistant Professor in 1981 at Osaka University where he was promoted to a Full Professor in 1994 and to a Distinguished Professor in 2013. His research has focussed on electron transfer chemistry, particularly artificial photosynthesis. He is currently a Distinguished Professor of Ewha Womans University (Korea), a Professor Emeritus of Osaka University and a Designated Professor of Meijo University (Japan).

Yong-Min Lee obtained his Ph.D. degree in Inorganic Chemistry at Pusan National University, Republic of Korea in 1999, under the supervision of Professor Sung-Nak Choi. From 1999 to 2005, he joined the Centro di Risonanze Magnetiche (CERM) at University of Florence (Italy) as a Postdoctoral fellow and Researcher under the supervision of Professors Ivano Bertini and Claudio Luchinat. Then, he moved to the Centre for Biomimetic Systems at Ewha Womans University, as a Research Professor (2006 -2009). He is currently a Special Appointment Professor at Ewha Womans University (2009 – present).

Wonwoo Nam obtained his B.S. (Honours) degree in Chemistry from California State University, Los Angeles, and his PhD degree in Inorganic Chemistry from University of California, Los Angeles (UCLA) under the supervision of Professor Joan S. Valentine in 1990. After working as a postdoctoral fellow at UCLA for one year, he became an Assistant Professor at Hong Ik University in 1991. In 1994, he moved to Ewha Womans University, where he is now a Distinguished Professor. His current research has focussed on the O_2 activation, water oxidation, metal-oxygen intermediates and important roles of metal ions in bioinorganic chemistry.

2. Ruthenium Complexes as WOCs

A dinuclear Ru(II) complex $[(bpy)_2(H_2O)RuORu(H_2O)\text{-}(bpy)_2]^{4+}$ (bpy = 2,2'-bipyridine), which is known as a blue dimer, was reported earlier as a homogeneous WOC by Meyer and co-workers in 1982.[134] Since then, a number of ruthenium complexes have been studied extensively as efficient and stable homogeneous WOCs.[135-140] Mononuclear Ru(II) complexes as well as dinuclear Ru(II) complexes act as homogeneous WOCs.[141-150] However, dinuclear Ru(II)-bpp complexes (bpp = 3,5-bis(pyridyl)pyrazolate) were reported to decompose in the course of the OER when the bpp ligands were oxidised to evolve CO_2.[139] The catalytic WOR activity was decreased by the ligand oxidation of mononuclear Ru(II) complexes with organic ligands.[145] In order to enhance the stability of Ru complexes during the OER, non-oxidisable inorganic ligands such as polyoxometalates (POMs) were employed instead of oxidisable organic ligands.[151-154] For example, a tetranuclear ruthenium polyoxometalate complex (Ru_4POM) was reported to act as an effective WOC with a turnover number (TON = 23) based on a ruthenium centre.[153,154] Mononuclear ruthenium complexes bearing Keggin-type lacunary heteropolytungstate, $[Ru^{III}(H_2O)SiW_{11}O_{39}]^{5-}$ (**1**) and $[Ru^{III}(H_2O)GeW_{11}O_{39}]^{5-}$ (**2**) (Fig. 1), were also reported to act as efficient and robust homogeneous catalysts for WOR by $(NH_4)_2[Ce^{IV}(NO_3)_6]$ (CAN).[155] Although CAN is not environmentally benign oxidant, CAN is useful for the mechanistic study. The oxygen atoms in the evolved O_2 were confirmed to originate from H_2O by carrying out isotope-labelling experiments using $H_2{}^{18}O$.[155]

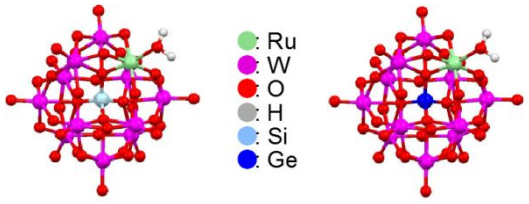

Fig. 1 Ball-and-stick structures of the polyanion complexes, $[Ru^{III}(H_2O)SiW_{11}O_{39}]^{5-}$ (**1**) and $[Ru^{III}(H_2O)GeW_{11}O_{39}]^{5-}$ (**2**). Reprinted with permission from reference 155. Copyright 2011, American Chemical Society.

Cyclic voltammograms of **1** and **2** exhibited three one-electron oxidation processes, all of which are chemically reversible.[157] Based on the pH dependence of the redox couples (Pourbaix diagrams), all the species at the different redox potentials and pH values can be identified (see Fig. 2).[155] The Ru^{IV}-OH_2 complex is formed at pH 1.0 at an applied potential between 0.62 and 0.90 V (*vs*. SCE) with no proton loss when the $E_{1/2}$ value is the same with the change in pH around 1.0 (Fig. 2).[155] In contrast, the Ru^{IV}-OH_2 complex is further oxidised to the Ru^{V}=O complex at pH 1.0 at an applied potential higher than 0.90 V with loss of two protons. The $E_{1/2}$ value decreases with increasing pH (> 1.0) with a slope = 118 mV/pH, which indicates $1e^-/2H^+$ process between pH 0 and 2.[155] Thus, at pH 1.0, **1** and **2** are oxidised by two equivalents of CAN ($E_{1/2}$ *vs*. SCE = 1.21 V) to produce $[Ru^{V}(O)SiW_{11}O_{39}]^{5-}$ and $[Ru^{V}(O)GeW_{11}O_{39}]^{5-}$, respectively.[155]

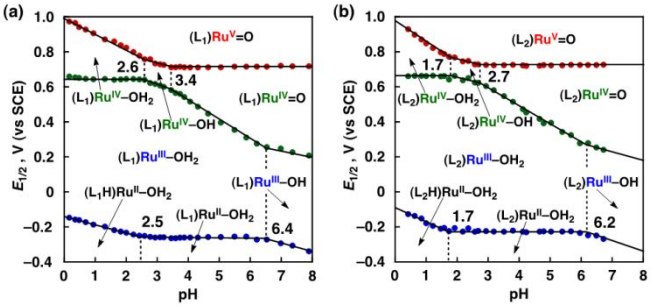

Fig. 2 Diagrams for $E_{1/2}$ of the $Ru^{III/II}$ (blue dots), $Ru^{IV/III}$ (green dots) and $Ru^{V/IV}$ (red dots) redox couples of (a) **1** ($L_1 = [SiW_{11}O_{39}]^{8-}$) and (b) **2** ($L_2 = [GeW_{11}O_{39}]^{8-}$).[155] All the p$K_a$ values are indicated by the vertical dashed lines. Reprinted with permission from reference 155. Copyright 2011, American Chemical Society.

The formation of the Ru^{IV}-OH_2 and the Ru^{V}=O species by stepwise oxidation of **1** by CAN was indicated by the corresponding stepwise absorption spectral change showing different isosbestic points for each step.[155] The formation of the Ru^{V}=O complexes produced in the reactions of **1** and **2** with two equivalents of CAN was confirmed by resonance Raman (rR) and electron paramagnetic resonance (EPR) measurements.[155] The

decay rates of CAN by the reactions with **1** and **2** obeyed the first-order kinetics with respect to initial concentrations of the catalysts, **1** and **2**.[155] If two Ru^{V}=O molecules are required for O-O bond formation in the OER, the rate would exhibit parabolic dependence with respect to the catalyst concentration (vide infra). Thus, the r.d.s. may be the nucleophilic attack of H_2O to the Ru^{V}=O complex for the O–O bond formation to produce the Ru^{III}-OOH species (Scheme 1)[155] as reported for other Ru WOCs.[156-158] According to Scheme 1, the rate of disappearance of Ce^{IV} (CAN) is given by eqn (1),

$$-d[Ce^{IV}]/dt = k_N k_{et}[Ru][H_2O]/(k_{-N}[H+] + k_{et}[Ce^{IV}]) \quad (1)$$

where k_N is the rate constant of the nucleophilic attack of H_2O to the Ru^{V}=O complex, k_{et} is the rate constant of electron transfer (ET) from the Ru^{III}-OOH complex to Ce^{IV}, and k_{-N} is the rate constant of the back reaction from the Ru^{III}-OOH complex with H^+ to regenerate the Ru^{V}=O complex.[155] Eqn (1) agrees with the observed first-order dependence of the WOR rate on the concentration of catalyst and the saturation dependence of the WOR on the pH and concentration of CAN.[155] The decay rate of CAN with **2** in the WOR was 1.5 times faster than that with **1**,[157] because of the electron-withdrawing effect of germanium, which is reflected in the smaller pK_a value of **2** than that of **1**.[155] The kinetic study (vide supra) clarifies the rate-determining step in the catalytic cycle in Scheme 1. However, the reaction intermediates proposed in Scheme 1 after the rate-determining step cannot be detected because of the much faster reactions after the rate-determining step. It is better to start the catalytic cycle from postulated intermediates to support the catalytic mechanism.

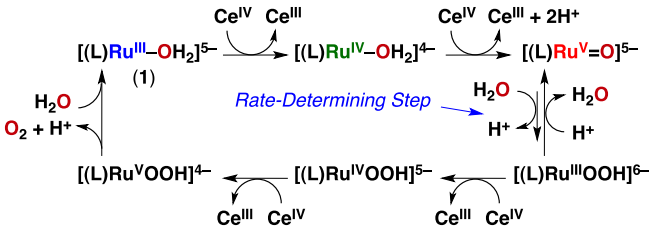

Scheme 1 Mechanism of WOR by Ru^{III}-OH_2 complexes (L = $[SiW_{11}O_{39}]^{8-}$ for **1** and $[GeW_{11}O_{39}]^{8-}$ for **2**) with CAN. Reprinted with permission from reference 155. Copyright 2011, American Chemical Society.

A seven-coordinate Ru^{V}=O intermediate of $[Ru(bda)(isq)_2]^{2+}$ (**3**: bda = 2,2'-bipyridine-6,6'-dicarboxylate, isq = isoquinoline) produced during the WOR was characterised by in situ extended X-ray absorption fine structure analysis, which indicates the Ru=O bond distance of 1.75 ± 0.02 Å, as predicted by the DFT calculations (Fig. 3).[159] The introduction of halogen and resulting in a lower activation energy to achieve a high TOF of 1270 s^{-1} for $[Ru(bda)(6\text{-OMe-isq})_2]$ (30 μM) in the catalytic WOR by CAN (0.365 M).[160] The rate of the consumption of CAN electron-donating substituents in $[Ru(bda)(6\text{-X-isq})_2]$ (X = H, F, Cl, Br and OMe) enhanced the non-covalent interactions between the axial ligands for the bimolecular O–O coupling, exhibited a second-order dependence on catalyst concentration [eqn (2)] at low concentrations of the Ru catalyst. Such a

$$-d[Ce^{IV}]/dt = k_{cat}[Ru]^2 \quad (2)$$

second-order dependence of the WOR rate on concentration of the Ru catalyst suggests that the bimolecular radical coupling of two Ru^{V}=O molecules for the O-O bond formation is the r.d.s., as proposed by Llobet, Sun and their co-workers (Scheme 2).[161-163]

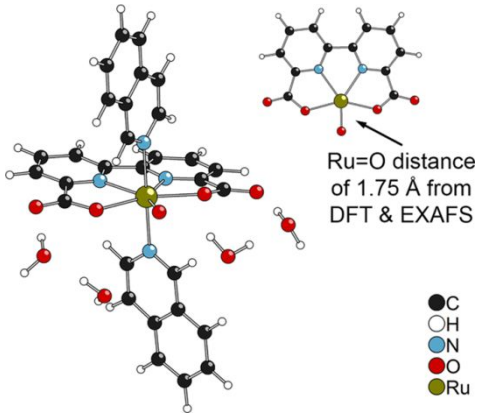

Fig. 3 (left) Calculated structure of $[Ru^{V}=O(bda)(isoq)_2]^+$ (**3**) with four solvated H_2O molecules. (right) Ru^{V}=O moiety with the equatorial tetradentate bda ligand. Reprinted with permission from reference 159. Copyright 2018, American Chemical Society.

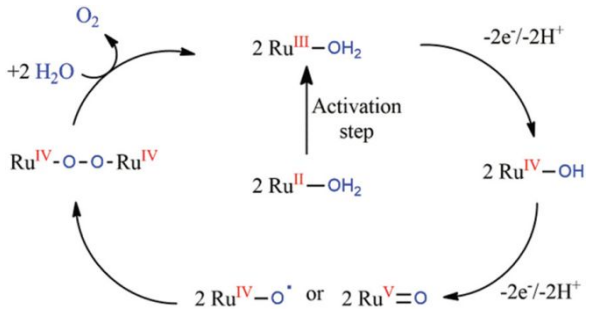

Scheme 2 Catalytic mechanism of WOR by CAN with $[Ru(bda)(6isq)_2]$ (**3**). Reprinted with permission from reference 163. Copyright 2016, Royal Society of Chemistry.

At higher concentrations of the Ru catalyst, the rate law was changed to the first order with respect to the catalyst concentration.[160,164] This indicates that the r.d.s. is changed from the bimolecular radical coupling of two Ru^{V}=O molecules to the subsequent mononuclear reaction step.[160] In such a case, the steady-state catalyst oxidation state during the WOR may be changed from Ru^{V}=O to Ru^{IV}-O-O-Ru^{IV} depending on the catalyst concentration. However, such a change of the oxidation state of the Ru catalyst under the steady-state conditions has yet to be clarified.

A seven-coordinate Ru^{V}=O intermediate of $[Ru^{V}(tda\text{-}\kappa\text{-}N^3O^1)(py)_2]^+$ (**4**: Fig. 4A) was reported to react with H_2O to produce $[Ru^{III}(OOH)(Htda\text{-}\kappa\text{-}N^2O^1)(py)_2]^+$ via the intramolecular proton transfer to the dangling carboxylate (Fig. 4B), which was further oxidised to evolve O_2.[158] Such an intramolecular proton transfer resulted in much enhancement of the catalytic activity

of **4** as indicated by TOF up to 8000 s^{-1} at pH 7.0 and 50,000 s^{-1} at pH 10 determined by a foot of the wave analysis of cyclic voltammograms, as compared with TOFs of the related complex ([Ru(bda)(Pic)$_2$]) without the dangling carboxylate (TOF = 6 S^{-1} at pH 7.0 and 14,000 s^{-1} at pH 12.2).[158] A $Ru^{V}(O)(t5_a\text{-}\kappa\text{-}N^2O)(py)_2$ complex ($t5_a^{3-}$ = 2,5-bis(6-carboxylatopyridin-2-yl)pyrrol-1-ide) also acts as a very efficient WOC, reaching the TOF_{MAX} value of 9400 s^{-1} at pH 7.0, which is among the highest ever reported at pH 7.0.[165]

There has been no report on the conversion of homogeneous ruthenium complexes to heterogeneous nanoparticle catalysts in the OER with CAN. However, ruthenium oxide (RuO_2) NPs are among the most active WOCs reported so far.[166-169] Whether Ru complexes with organic ligands are converted to RuO_2 NPs during the WORs should be checked with much caution by using various techniques (vide infra).

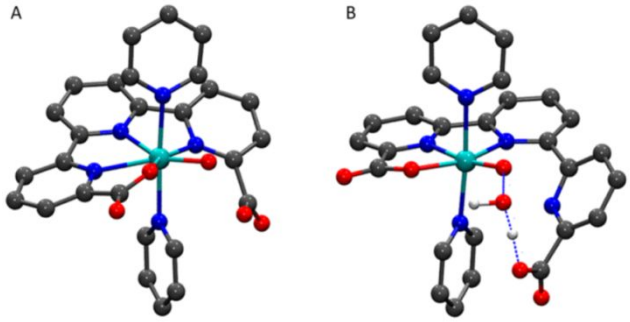

Fig. 4 Optimized structures of (A) $[Ru^{V}(tda\text{-}\kappa\text{-}N^3O^1)(py)_2(O)]^+$ (**4**) and (B) the calculated transition state produced in the nucleophilic attack of water to the $Ru^{V}(O)$ species at the M11-L level of theory [Ru (cyan), C (gray), N (deep blue), O (red) and H (white)]. Reprinted with permission from reference 158. Copyright 2015, American Chemical Society.

3. Metal Complex Precursors to Metal Nanoparticle WOCs

3.1. Iridium Complexes

Not only ruthenium oxides but also iridium oxides are efficient heterogeneous WOCs.[170-174] Molecular iridium complexes were reported to act as homogeneous WOCs.[175-184] However, the Cp* ligand of $[Cp^*Ir(H_2O)_3](SO_4)$ and $[(Cp^*Ir)_2(OH)_3](OH)$ (Cp* = pentamethylcyclopentadienyl) was oxidised electrochemically to produce an amorphous iridium oxide (IrO_x) layer containing a carbon admixture deposited onto the anode, which acted as a more active and robust WOC for the electrochemical WOR.[185-189] Such a change from molecular Ir complexes to IrO_x NPs as true WOCs was also observed in catalytic WOR by CAN (vide infra).[190,191]

Time courses of the rate of WOR by CAN with Ir(III) complexes, $[Ir^{III}(Cp^*)(4,4'\text{-}R_2\text{-}2,2'\text{-}bpy)(H_2O)](SO_4)$ [R = OH (**5**), OMe (**6**), Me (**7**) and COOH (**8**)] (Fig. 5) in the presence of HNO_3 (0.10 M) in H_2O are shown in Fig. 6a, where the turnover frequency (TOF) is plotted against reaction time.[191] The TOF was determined from the initial decay rate of CAN divided by four (= $-d[Ce^{IV}]/dt)/4$) according to the stoichiometry of the WOR by Ce^{IV} (CAN) [eqn (3)]. The TOF of the WOR with **6** – **8** decreased with reaction time, whereas the TOF with **5** increased with time to reach a highest value at 900 s. After the maximum value, the TOF decreased as the CAN was consumed at 1100 s.[191] It was confirmed that the evolved O_2 originated from H_2O by performing isotope-labelling experiments using $H_2{}^{18}O$.[191] The observed increase in TOF with reaction time indicates that **5** acts as a precursor for the more reactive catalyst for the WOR by CAN.[191] After all CAN molecules were consumed in the WOR in the 1st cycle, addition of another batch of CAN to the resulting solution started the 2nd cycle. The TOF value at the beginning of the 2nd cycle was virtually the same as the largest value in the 1st cycle as shown in Fig. 6b, where the catalytic activity also remained the same in the 3rd cycle.[191] This indicates that **5** was converted to the active and robust catalyst during the 1st cycle of the WOR.

$$2H_2O + 4Ce^{IV} \xrightarrow[cat]{} O_2 + 4H^+ + 4Ce^{III} \quad (3)$$

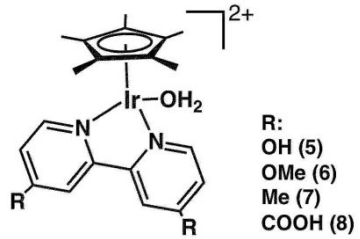

Fig. 5 Mononuclear $[Ir^{III}(Cp^*)(H_2O)]^{2+}$ derivatives employed as precursors of a true WOC in the catalytic WOR by CAN. Reprinted with permission from reference 191. Copyright 2012, Royal Society of Chemistry.

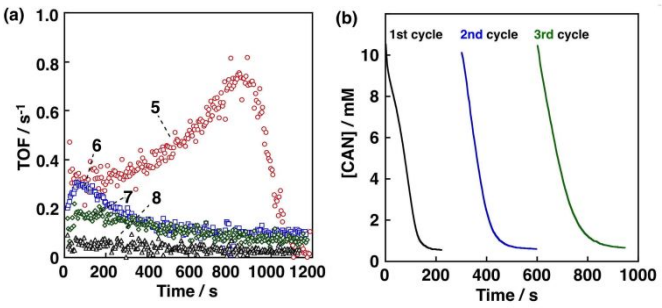

Fig. 6 (a) Time courses of TOF of WOR by CAN (10 mM) with iridium complexes [**5**, **6**, **7** and **8**] in the presence of HNO_3 (100 mM) in H_2O. (b) Time profiles of the decay of CAN in the catalytic WOR by CAN (10 mM) with the precursor **5** (50 μM) in the presence of HNO_3 (100 mM) in H_2O (2.0 mL) for the 1st, 2nd and 3rd cycles. Reprinted with permission from reference 191. Copyright 2012, Royal Society of Chemistry.

Dynamic light scattering (DLS) measurements were performed to confirm the formation of NPs during the catalytic WOR by CAN with **5** as shown in Fig. 7, where the size of NPs increased with increasing concentration of the precursor **5**.[191] The size of NPs was in the rage of 100 – 300 nm, as shown by the transmission electron microscope (TEM) images in Fig. 8.[191]

X-ray photoelectron spectroscopy (XPS) is a surface-sensitive quantitative spectroscopic technique and the XPS spectra of NPs formed in the catalytic WOR by CAN with **5** (Fig. 9) indicate that the Ir $4f_{5/2}$ peak of the NPs appeared at 62.8 eV shifted by –0.9 eV in reference to the Ir $4f_{5/2}$ peak of IrO_2 NPs.[191] The peak of oxygen 1s of the NPs (532.3 eV) also shifted to be higher than

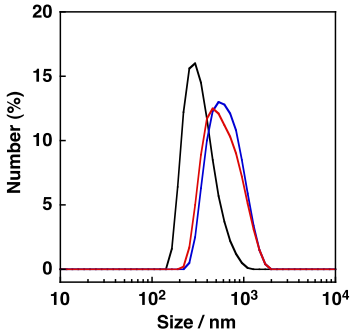

Fig. 7 Dynamic light scattering (DLS) data of aqueous solutions of **5** (black line: 50 μM, blue line: 250 μM and red line: 500 μM), CAN (10 mM) and HNO_3 (100 mM). Reprinted with permission from reference 191. Copyright 2012, Royal Society of Chemistry.

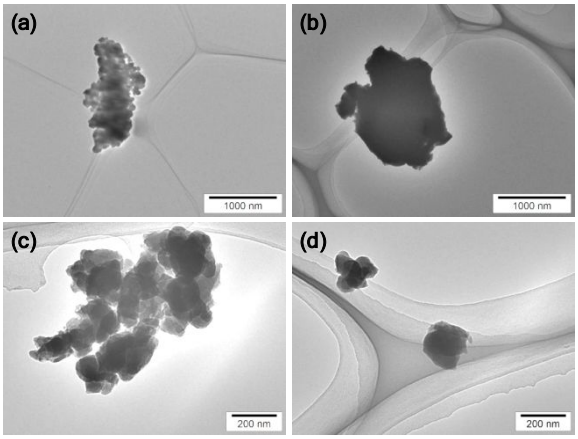

Fig. 8 TEM images of NPs produced in the catalytic WOR by CAN with **5** at different magnifications (a–d). Reprinted with permission from reference 191. Copyright 2012, Royal Society of Chemistry.

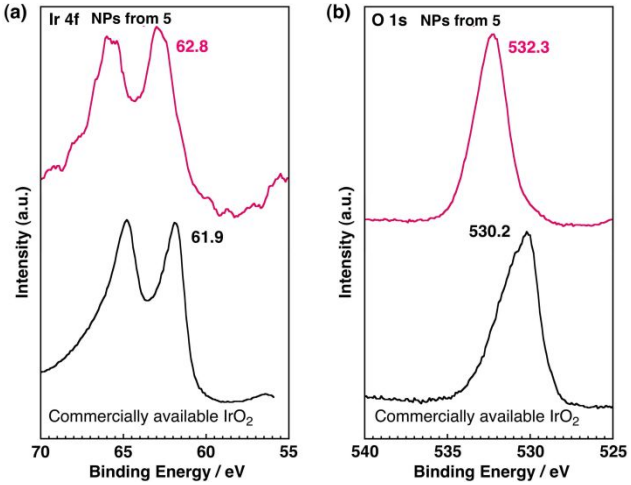

Fig. 9 XPS spectra of NPs derived from **5** in the WOR by CAN and commercially available IrO_2 (reference) in the region of the binding energy of (a) Ir 4f and (b) oxygen 1s. Reprinted with permission from reference 191. Copyright 2012, Royal Society of Chemistry.

that of the reference IrO_2 NPs (530.2 eV).[191] Such a shift of the oxygen 1s peak suggests the formation of iridium hydroxide species ($Ir(OH)_x$).[192,193] Thermogravimetry/differential thermal analysis (TG/DTA) measurements also supported the formation of $Ir(OH)_3$ from **5** because the weight loss corresponded to the thermal dehydration reaction from $Ir(OH)_3$ to IrO_2.[191] Thus, NPs derived from **5** after the catalytic WOR by CAN consist of $Ir(OH)_x$ (x = 3) and carbonaceous residues.[191]

The facile conversion of **5** to $Ir(OH)_x$ NPs in the catalytic WOR by CAN as compared with **6** – **8** suggests that the ligand of **5** was much easily oxidised by CAN than those of **6** – **8**. In fact, the [4,4'-$(OH)_2$-bpy] ligand of **5** showed the higher reactivity in oxidation by CAN to produce CO_2 as compared with the ligands of **6** – **8**.[191]

Organometallic iridium complexes (**9** – **14**) in Fig. 10 were also converted to NPs, which act as true catalysts during the catalytic WOR by CAN.[194] $IrCl_3$ without any organic ligands also acts as a precursor of NPs in the catalytic WOR by CAN.[194] However, it was reported that homogeneous Ir(IV) complexes existed during the catalytic WOR by $NaIO_4$ under various pH conditions.[195,196] A molecular Ir monolayer of the catalyst exhibited higher activity than the bulk material analogue, IrO_x.[197] It was also reported that both molecular Ir complexes and IrO_x NPs existed in the WOR determined by *in situ* X-ray absorption spectroscopy.[198] Whether heterogeneous IrO_x NPs were formed from Ir complexes or Ir complexes remain as homogeneous catalysts is changed depending on supporting organic ligands, concentrations of Ir complexes, the type of employed oxidants, pH and temperature.[199-204]

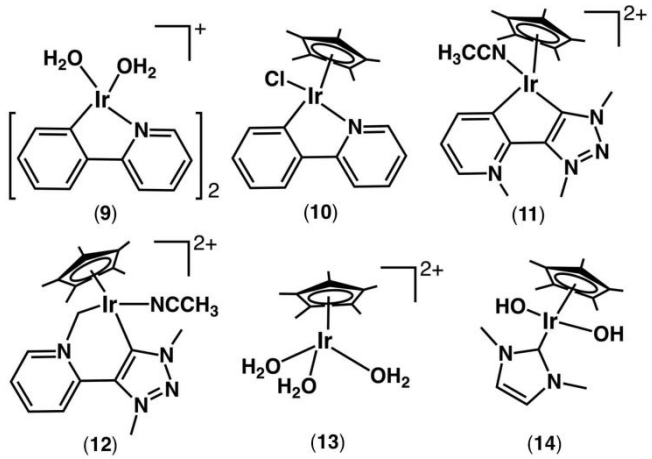

Fig. 10 Ir complexes employed as precursors of NPs during the catalytic WOR by CAN. Reprinted with permission from reference 194. Copyright 2011, American Chemical Society.

3.2. Cobalt Complexes

It is desired to develop WOCs using earth-abundant metals rather than Ru and Ir, and a robust heterogeneous WOC was reported using cobalt phosphate.[205-208] A homogeneous tetranuclear cobalt complex, $[Co_4(H_2O)_2(PW_9O_{34})_2]^{10-}$ (Co_4POM (**15**) in Fig. 11a), composed of a Co_4O_4 core stabilized by non-oxidisable polytungstate ligands, was used as a robust WOC in the catalytic WOR by $[Ru(bpy)]_3^{3+}$ at pH 8.0.[209] Since $[Ru(bpy)_3]^{3+}$ is formed by oxidative quenching of the excited state of $[Ru(bpy)_3]^{2+}$ ($[Ru(bpy)_3]^{2+*}$: * denotes the excited state) by $S_2O_8^{2-}$,[210] H_2O can be oxidised by $[Ru(bpy)]_3^{3+}$ to evolve O_2 using

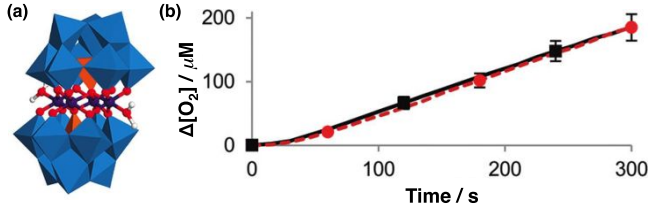

Fig. 11 (a) Structure of $[Co_4(H_2O)_2(PW_9O_{34})_2]^{10-}$ (**15**: Co_4POM).[209,214] (b) Time profiles of O_2 evolution ($\Delta[O_2] = [O_2]_t - [O_2]_{t=0}$) during the controlled-potential electrolysis of a phosphate buffer solution (pH 8.0) containing 500 μM Co_4POM (red cycle) or 58 μM $Co(NO_3)_2$ (black square) at an applied potential of 1.1 V *vs*. Ag/AgCl. Reprinted with permission from reference 214. Copyright 2011, American Chemical Society.

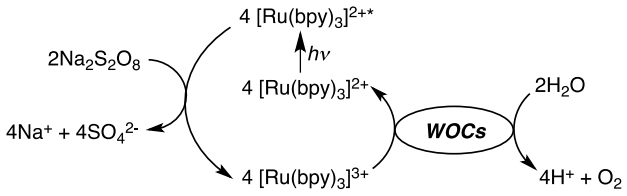

Scheme 3 Catalytic cycle of photochemical WOR with $Na_2S_2O_8$ and $[Ru(bpy)_3]^{2+}$ using WOCs. Reprinted with permission from reference 210. Copyright 2002, American Chemical Society.

WOCs under photoirradiation as shown in Scheme 3. Electron transfer from $[Ru(bpy)_3]^{2+*}$ to $S_2O_8^{2-}$ produces $[Ru(bpy)_3]^{3+}$, $SO_4^{2-}$and $SO_4^{\bullet-}$. The oxidising ability of $SO_4^{\bullet-}$ produced in the photoinduced ET is strong enough [$E^0(SO_4^{\bullet-}/SO_4^{2-}) = 2.6$ V][211] to oxidise $[Ru(bpy)_3]^{2+}$ thermally to produce two equivalents of $[Ru(bpy)_3]^{3+}$ in the photocatalytic WOR. When **15** was used as a WOC, the yield of O_2 produced was determined to be 45% based on the initial concentration of $Na_2S_2O_8$ ($2[O_2]_f/[Na_2S_2O_8]_0$; $[O_2]_f$ is the final O_2 concentration) with the initial quantum yield of 30%.[212] The O_2 yield was improved to 60% when $K_7[Co^{III}Co^{II}(H_2O)W_{11}O_{39}]$ was employed as a WOC.[213]

Co_4POM (**15**) was stable and no NPs were formed under photocatalytic WOR in Scheme 3.[209,212] However, **15** was reported to be converted to active cobalt oxide NPs at pH 8.0 by releasing Co(II) during the electrocatalytic WOR.[214] As shown in Fig. 11b, the time profile of the electrocatalytic O_2 evolution with **15** (500 μM) is identical to that with $Co(NO_3)_2$ (58 μM) during the controlled-potential electrolysis at 1.1 V *vs*. Ag/AgCl (pH 8.0).[214] Such agreement suggests that the Co^{2+} ions leached from the Co_4POM solution are converted to CoO_x NPs that act as a true WOC for the electrocatalytic WOR.[214] Depending on pH, water-soluble cobalt-polyoxometalate (Co-POM) complexes were changed to act as either a homogeneous catalyst or a heterogeneous catalyst for electrocatalytic and photocatalytic WOR.[215-217] In contrast to water soluble Co-POMs, a water insoluble salt of $[Co_9(H_2O)_6(OH)_3(HPO_4)_2(PW_9O_{34})_3]^{16-}$ (Co_9POM) was reported to act as a heterogeneous WOC exhibiting remarkable long-term stability in the solid state.[218] The barium salt of Co_9POM outperforms the state-of-the-art IrO_2 catalyst even at pH < 1, with an overpotential of 189 mV at 1 mA cm^{-2}.[219] The catalytic stability in acidic media was enhanced by using a carbon-paste conducting support with a hydrocarbon binder, which provides a hydrophobic environment.[219]

Water-soluble cobalt complexes with organic ligands, $[Co^{II}(Me_6tren)(OH_2)]^{2+}$ (**16**), $[Co^{III}Cp^*(bpy)(OH_2)]^{2+}$ (**17**), $[Co^{II}$(12-TMC)$]^{2+}$ (**18**) or $[Co^{II}$(13-TMC)$]^{2+}$ (**19**) (Me_6tren = tris(*N*,*N*'-dimethylaminoethyl)amine, 12-TMC = 1,4,7,10-tetramethyl-1,4,7,10-tetraaza-cyclododecane and 13-TMC = 1,4,7,10-tetramethyl-1,4,7,10-tetraa-zacyclotridecane) (Fig. 12), were converted to NPs that act as a true catalyst for photocatalytic WOR by $Na_2S_2O_8$ with $[Ru(bpy)_3]^{2+}$.[220] The O_2 yields in the photocatalytic WOR with **16**, **17**, **18** and **19** at pH 8.0 were also determined to be 54, 29, 16 and 41%, respectively. The quantum yields of O_2 evolution with **16** and **17** at pH 8.0 were determined to be 32 and 30%, respectively.[220] The oxygen atoms of evolved O_2 were confirmed to originate exclusively from H_2O by isotope-labelling experiments using $H_2{}^{18}O$.[220]

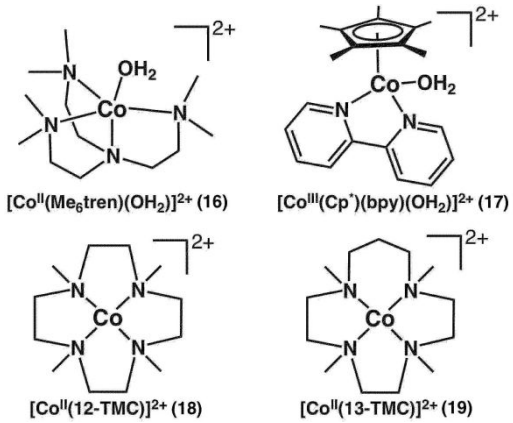

Fig. 12 Co(II) macrocyclic complexes employed as precursors of NPs catalysts for the photocatalytic WOR. Reprinted with permission from reference 220. Copyright 2012, Royal Society of Chemistry.

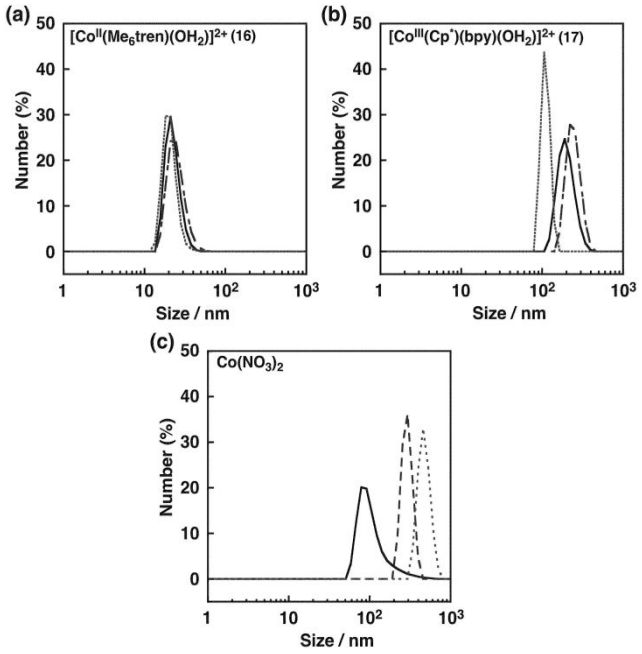

Fig. 13 DLS data of NPs formed from (a) **16**, (b) **17** and (c) $Co(NO_3)_2$. NPs were produced by photoillumination of a borate (100 mM) buffer solution (pH 9.0) of **16**, **17** or $Co(NO_3)_2$ (50 μM), $[Ru(bpy)_3]^{2+}$ (0.50 mM) and $Na_2S_2O_8$ (10 mM)

with a Xe lamp (λ > 420 nm) for 3 min (black line), 10 min (broken line) and 30 min (dotted line). Reprinted with permission from reference 220. Copyright 2012, Royal Society of Chemistry.

Photoillumination of an aqueous solution of **16** (50 μM), $[Ru(bpy)_3]^{2+}$ (0.50 mM) and $Na_2S_2O_8$ (10 mM) with visible light (λ > 420 nm) at pH 9.0 for 3 min resulted in the formation of NPs with the size of ca. 20 nm as detected by DLS measurements (Fig. 13a). The size of NPs produced from **17** was larger in the range of 100 - 500 nm, which became larger at a longer photoillumination time (Fig. 13b).[220] The size of NPs produced from $Co(NO_3)_2$ (50 μM) also increased to ca. 500 nm by elongation of the photoillumination time up to 30 min as shown in Fig. 13c.[220] These results indicate that NPs are produced from **16**, **17** and $Co(NO_3)_2$ at the early stage of the photocatalytic WOR by $Na_2S_2O_8$ with $[Ru(bpy)_3]^{2+}$.[220] TEM images of the NPs formed from **16**, **17** and $Co(NO_3)_2$ agree with the particle size estimated by DLS measurements.[220]

X-ray photoelectron spectra (XPS) of the NPs formed in the photocatalytic WOR by $Na_2S_2O_8$ with **16** are shown in Fig. 14, where the NPs formed from **16** revealed two intense peaks at 780.0 eV for Co $2p_{1/2}$ and 795.3 eV for Co $2p_{3/2}$ with weak satellite peaks, whereas Co_3O_4 exhibits two strong peaks at 779.8 eV for Co $2p_{3/2}$ and at 795.1 eV for Co $2p_{1/2}$ with small satellite peaks as well.[220] The satellite peaks observed for the NPs are assigned due to the higher ratio of Co(II) species compared with the authentic Co_3O_4 sample. The oxygen 1s peak of the NPs was observed at 531.5 eV, which is by 1.2 eV higher than the oxygen 1s peak of Co_3O_4 (530.3 eV). The higher energy of the oxygen 1s peak of the NPs was reported to result from metal hydroxide species.[220] Thus, the surface of the NPs converted from **16** under the photocatalytic WOR by $Na_2S_2O_8$ consists of $Co(OH)_x$ that acts as the true WOC for the photocatalytic WOR. TG/DTA measurements indicated the existence of carbonaceous residues in the NPs produced via the oxidation of Me_6tren ligand of **16**.[220] Cobalt NPs produced *in situ* from Co^{2+} ions and methylene diphosphonate in the photocatalytic WOR also exhibited a high catalytic reactivity.[221]

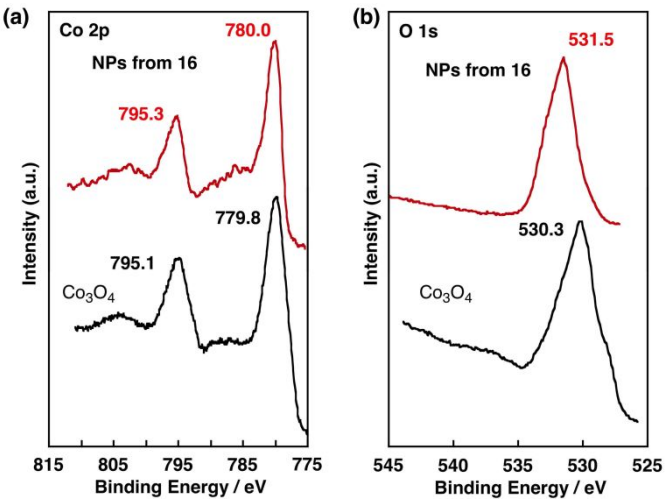

Fig. 14 XPS spectra of NPs formed from **16** (red) and Co_3O_4 (black) in the binding energy regions of (a) Co 2p and (b) oxygen 1s. Reprinted with permission from reference 220. Copyright 2012, Royal Society of Chemistry.

Although **17** was converted to $Co(OH)_x$ NPs in the photocatalytic WOR by $Na_2S_2O_8$ under alkaline conditions (vide supra),[220] **17** was reported to act as a homogeneous WOC under acidic conditions with $Sc(NO_3)_3$ (100 mM), combined with photocatalytic two-electron reduction of O_2 for overall WRC to produce H_2O_2.[222-224]

In contrast to the case of **16**-**19**, a dinuclear bis-μ-hydroxo Co^{III}(TPA) complex [**20**: $[(TPA)Co(\mu\text{-}OH)_2Co(TPA)](ClO_4)_3$ (TPA = tris(2-pyridylmethyl)amine) in Fig. 15] was reported to act as a homogeneous WOC in photocatalytic WOR by $Na_2S_2O_8$ with $[Ru(bpy)_3]^{2+}$ in borate buffer (pH 8.0).[225,226] At pH 9, **20** is deprotonated to produce the μ-oxo-μ-hydroxo dinuclear Co^{III} complex, $[Co^{III}_2(\mu\text{-}O)(\mu\text{-}OH)(TPA)_2]^{3+}$ (**20**-H^+).[226] The two-electron oxidation of $[Co^{III}_2(\mu\text{-}O)(\mu\text{-}OH)(TPA)_2]^{3+}$ by two

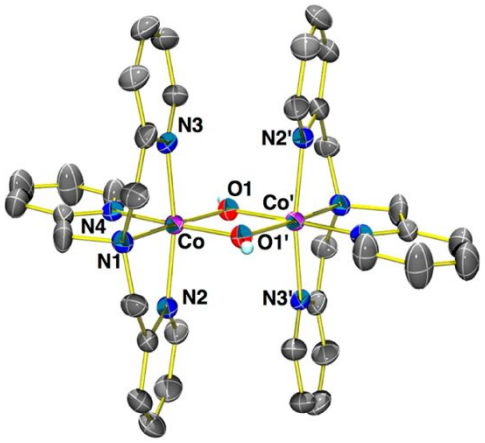

Fig. 15 X-ray crystal structure of a bis-μ-hydroxo Co^{III}(TPA) complex (**20**). Reprinted with permission from reference 226. Copyright 2016, American Chemical Society.

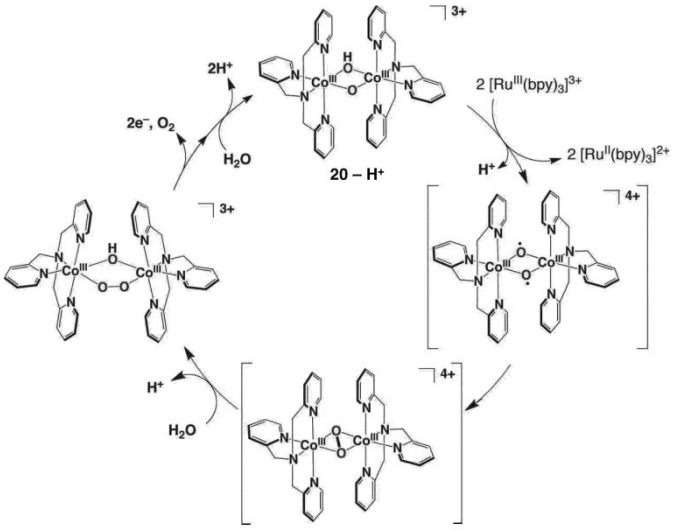

Scheme 4 Catalytic mechanism of WOR by $[Ru(bpy)_3]^{3+}$ with **20** used as

a WOC in a B-R buffer at pH 8. Reprinted with permission from reference 226. Copyright 2016, American Chemical Society.

equivalents of $[Ru(bpy)_3]^{3+}$ affords the triplet bis-μ-oxyl complex after removal of proton, which is proposed to undergo a spin flip to give a singlet bis-μ-oxyl complex, followed by intramolecular radical coupling between the two oxyl ligands to produce a μ:η^2,η^2-peroxo dinuclear Co^{III} intermediate (Scheme 4).[226] The reaction of the μ:η^2,η^2-peroxo dinuclear Co^{III} intermediate with water yields a μ-peroxo-μ-hydroxo dinuclear Co^{III} complex, which is further oxidised by two equivalents of $[Ru(bpy)_3]^{3+}$ to evolve O_2, accompanied by regeneration of **20-H$^+$**.[226] The r.d.s. is suggested to be initial proton-coupled electron transfer from **20-H$^+$** to $[Ru(bpy)_3]^{3+}$, precluding the detection of the reactive intermediates in the catalytic cycle in Scheme 4.[226]

On the other hand, EDTA and 2,2'-bipyridine titrations together with scanning electron microscopy (SEM), EDX, ICP-AES, TEM and XPS measurements revealed that **20** is a precursor for CoO_x NPs that act as a true WOC.[227] After the photocatalytic WOR with **20**, the solution was taken on the Cu grid to observe traces of CoO_x by TEM.[227] When a magnetic stirring bar was used during the photocatalytic WOR, no heterogeneous CoO_x could be observed by TEM, because the produced CoO_x adhered on the surface of the magnetic stirring bar.[227] The presence of CoO_x formed in the photocatalytic WOR would be difficult to detect by DLS measurements.[227] At a high concentration (1 mM), however, the dinuclear Co catalyst remained intact after the photocatalytic WOR as revealed by the ^{1}H NMR measurements.[226] Thus, whether WOCs are homogeneous or heterogeneous may depend on concentrations of catalysts.

Mononuclear cobalt(III) complexes with tetraamido macrocyclic ligands (Na[(TAML)Co^{III}] (**21**): TAML = 3,3,6,6,9,9-hexametyl-2,5,7,10-tetraoxo-3,5,6,7,9,10-hexahydro-2*H*-benzo[*e*][1,4,7,10]-tetraazacyclotridecine-1,4,8,11-tetraide and (Et_4N[(bTAML)Co^{III}] (**22**): bTAML = biuret-modified tetraamidomacrocyclic) in Fig. 16) were found to act as stable and efficient homogeneous catalysts for electrocatalytic WOR in phosphate buffer.[228,229] In 0.10 M phosphate buffer at pH 9.2, CV responses of **22** (0.25 mM) exhibited two irreversible oxidation waves at $E_{p,a}$ *vs.* NHE = 1.1 V and second at $E_{p,a}$ *vs.* NHE = 1.5 V with an enhanced current above the background, indicating a catalytic process.[229] In 0.1 M deuterated phosphate buffer at pD = 9.2, the first irreversible wave was shifted by 0.2 V to afford the deuterium kinetic isotope effect (KIE = 8.63), while the second wave remained constant.[229] Such a large KIE indicates that the first irreversible wave is associated with a concerted proton–electron transfer (CPET) process to produce the Co^{IV}(O) species [eqn (4)].[229] On the other hand, the second wave is a pH independent ET process to produce the Co^{V}(O) species [eqn (5)].[229]

$$[(bTAML)Co^{III}]^- + H_2O - e^- \rightarrow [(bTAML)Co^{IV}(O)] + 2H^+ \quad (4)$$

$$[(bTAML)Co^{IV}(O)] - e^- \rightarrow [(bTAML)Co^{V}(O)]^+ \quad (5)$$

Due to the redox non-innocent nature of the TAML igand,[230] the Co^{IV}(O) and Co^{V}(O) species may be better described as $[(bTAML^{\bullet+})Co^{III}(O)]$ or $[(bTAML^{2+})Co^{III}(O)]$, respectively. The electron-transfer oxidation of **21** by one-electron oxidants such as copper(II) triflate, $[Fe^{III}(bpy)_3]^{3+}$, tris(4-bromophenyl)ammoniumyl radical cation and CAN (E_{red} = 1.4 V *vs.* SCE) with H_2O resulted in formation of $[(TAML)Co^{IV}(O)]^{2-}$ that was detected by EPR.[231,232] In any case, the two-electron oxidised species is likely the key intermediate responsible for O–O bond formation in the WOR catalytic cycle as the case of the Ru^{V}(O) species in Scheme 1.[229]

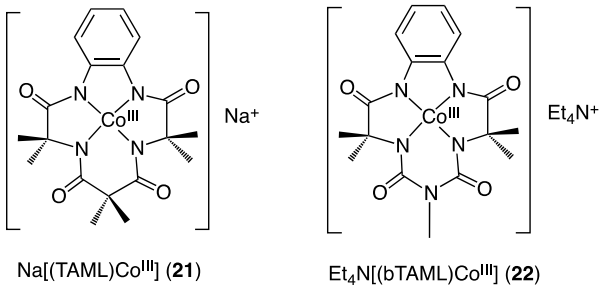

Fig. 16 Cobalt(III) complexes with tetraamido macrocyclic ligands (**21**: Na[(TAML)Co^{III}] and **22**: Et_4N[(bTAML)Co^{III}]) used for electrocatalytic WOR in phosphate buffer. Reprinted with permission from reference 228. Copyright 2018, American Chemical Society.

The O_2 evolution was confirmed by bulk electrolysis at +1.40 V (*vs.* Ag/AgCl) on an ITO electrode with a large surface area (1 cm^2) and using **21** (1 mM) in phosphate buffer (pH 7.0) as shown in Fig. 17 (blue line), where an induction period was observed for O_2 evolution.[228] It was confirmed that O_2 evolution was negligible without **21** (black line).[228] Although the Faraday efficiency of O_2 evolution was higher than 90%, the O_2 yield (250 μM) at 4000 s was much smaller the catalyst concentration (1 mM) with the TON of smaller than 1.[228] The induction period may indicate the formation of heterogeneous CoO_x that may be much more active than the starting homogeneous catalyst. However, the X-ray photoelectron spectroscopic (XPS) measurements exhibited no signal due to CoO_x formed on the ITO electrode after bulk electrolysis.[228,229] SEM of the ITO surface topography also indicated that no CoO_x was precipitated during the electrolysis.[228,229] Whether **21** and **22** act as homogeneous WOCs or precursors of heterogeneous NPs catalysts should also be checked for homogeneous photocatalytic WOR by $Na_2S_2O_8$ with $[Ru(bpy)_3]^{2+}$.

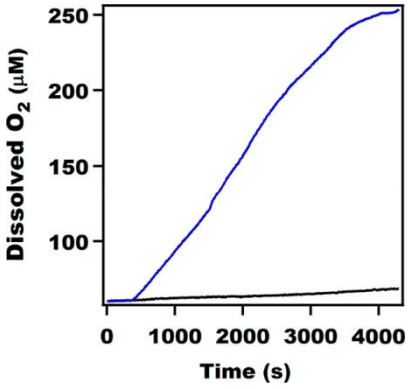

Fig. 17 Time profile of O_2 evolution in the course of bulk electrolysis of a 0.10 M phosphate buffer solution (pH 7.0) of 1.0 mM Na[(TAML)Co^{III}] (**21**) at an applied potential of 1.40 V *vs*. Ag/AgCl on the ITO electrode (1.0 cm^2). Reprinted with permission from reference 228. Copyright 2018, American Chemical Society.

Cobalt porphyrins and corroles were also reported to act as efficient homogeneous catalysts for WOR under basic conditions.[233-238] However, combination of electrochemistry, UV-vis, SEM, energy-dispersive X-ray spectroscopy (EDS), and synchrotron-based photoelectron spectroscopy (SOXPES and HAXPES) indicated that cobalt porphyrins, which were deposited on FTO glasses, were readily decomposed into a thin film of CoO_x on the surface of the electrode during the electrocatalytic WOR in a borate buffer solution (pH 9.2).[239] The UV-vis, SEM, EDS measurements are not sensitive enough for detection of CoO_x on the FTO electrode.[239] In order to detect CoO_x on the FTO electrode, adjusting the photon energy of the XPS to 1000 eV (SOXPES) was crucial in order to provide high surface sensitivity.[239] A high TOF of 10 s^{-1} was obtained for the electrocatalytic oxidation of water using the CoO_x/FTO electrode derived from cobalt porphyrins.[239]

3.3. Manganese Complexes

Manganese complexes have been extensively studied as functional mimics of the OEC in PSII in the past decades.[240-246] For example, a dinuclear manganese complex, $[Mn_2(OAc)_2(bpmp)]^+$ (bpmp = 2,6-bis[{*N*,*N*-di(2-pyridylmethyl)amino}methyl]-4-methylphenol anion), was reported to act as a homogeneous catalyst for WOR by oxone (HSO_5^-) to evolve O_2 together with CO_2 due to ligand oxidation.[247] In this reaction, manganese complexes (**23** and **24** shown in Fig. 18) were converted to manganese oxide (MnO_x) NPs as a true catalyst during the catalytic WOR by CAN.[248] The MnO_x NPs were characterised by XPS, EPR, FTIR, TEM, SEM and XRD measurements.[248]

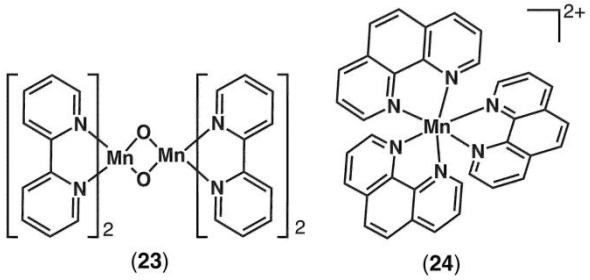

(**23**) (**24**)

Fig. 18 Manganese complexes used as precursors for the catalytic WOR by CAN.[248]

Highly dispersed MnO_x NPs with the size of 10 – 20 nm and 6 – 10 nm were also produced from $[Mn(Me_3TACN)(OMe)_3]^+$ and $[(Me_3TACN)_2Mn^{III}_2(\mu\text{-}O)(\mu\text{-}CH_3COO)_2]^{2+}$ (Me_3TACN = *N*,*N*',*N*''-trimethyl-1,4,7-triazacyclononane), respectively, via the dissociation of the complexes into Mn(II) species that were oxidised by applying an external bias potential.[249] The electrochemical oxidation of $[Mn(OH_2)_6]^{2+}$ also resulted in generation of MnO_x NPs with the size of 30 – 100 nm, which were less active WOCs.[249] A TOF of more than 100 molecules of O_2 Mn^{-1} s^{-1} was achieved for MnO_x NPs with the smaller size of ca. 10 nm.[249]

A water-soluble Mn-K cluster, $[Mn_8K_2(\mu\text{-}O)4(\mu\text{-}OH)_2(Piv)_{16}(Piv\text{–}H)(CH_3CN)]$ (Piv-H = pivalic acid), was also converted to MnO_x NPs, which were characterised by using X-ray absorption spectroscopy (XPS), SEM, TEM, FTIR, X-ray diffraction and electrochemical methods.[250] MnO_x NPs thus produced act as true catalysts for electrocatalytic WOR.[250]

Molecular catalysis for WOR was recently reported for manganese porphyrin dimers with mono- and hexaphosphonic acid groups ($Mn_2DP\text{-}PO_3H_2$ and $Mn_2DP\text{-}(PO_3H_2)_6$), which were covalently assembled on the surface of ITO electrode (ITO = indium-doped tin oxide). The $Mn_2DP\text{-}PO_3H_2$/ITO assemblies showed high TOFs (up to 47.4 s^{-1}) at a low overpotential (η = 0.26 V) at pH 1.5.[251] The robustness of the catalyst was much improved when $Mn_2DP\text{-}(PO_3H2)_6$/ITO assemblies were used as the WOC by the sake of the increased number of phosphonic acid anchor groups.[251] The $Mn^V(O)$ species were proposed to be the reactive intermediate for the WOR to form the O-O bond by the nucleophilic attack of water as the case of the $Ru^V(O)$ species in Scheme 1.[251] It was demonstrated that the addition reaction of hydroxide ion to the $Mn^V(O)$ species derived from the manganese(III) corrole complexes, $[(TPFC)Mn^{III}]$ (TPFC = 5,10,15-tris(pentafluorophenyl)corrolato trianion), afforded the Mn^{IV}-peroxo species via O–O bond formation and the resulting Mn^{IV}-peroxo species reverted to the $Mn^V(O)$ species upon addition of proton, indicating that the O-O bond formation and cleavage reactions between the $Mn^V(O)$ and Mn^{IV}-peroxo complexes were reversible.[252-254] On the basis of hybrid density functional calculations, however, the crucial O–O bond formation proceeds from the formal $Mn_4{}^{IV,IV,IV,V}$ state of a tetranuclear Mn complex by direct coupling of a Mn^{IV}-bound terminal oxyl radical and a di-Mn bridging oxo group,[255] a mechanism quite similar to that proposed for the natural system.[256]

3.4. Iron Complexes

Extensive efforts have been made to develop efficient WOCs composed of more earth-abundant metals than Co, such as Mn,[240-254] Ni,[257-261] Cu,[262-271] and Fe[272-276] (vide infra). Among earth-abundant metals, Fe is the most earth-abundant and environmentally friendly metal, which is commonly employed as catalysts for organic substrate oxidation by metalloenzymes and metal catalysts.[277-283] Mononuclear Fe complexes with tetradentate N donor ligands containing H_2O coordination sites (**25** and **26** in Fig. 19) exhibited high catalytic activity for WOR by CAN with a maximum TON values of 360 and 145 with **25** and **26**, respectively, at pH 1.0.[284] The TON value is limited by the demetallation associated with the ligand dissociation of the iron

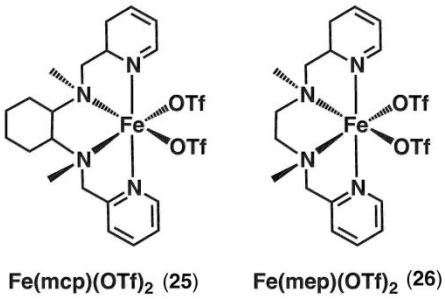

Fig. 19 Fe(II) complexes with tetradentate N donor ligands (**25** and **26**) employed for thermal and photochemical WORs.[284]

complexes under acidic conditions, and the dissociated ligands were oxidised by CAN to yield CO_2.[284,285] In competition with the ligand oxidation, the iron(IV)-oxo species was produced as the reactive intermediate for the O-O bond formation in the catalytic WOR, being detected by UV-vis absorption and electrospray ionization mass spectrometer (ESI-MS) measurements.[284] DLS measurements and NP-tracking analysis (NTA) indicated no appreciable formation of iron oxide NPs when **25** acted as a homogeneous WOC during the WOR.[284]

Other iron complexes, such as $[Fe(bpy)_2Cl_2]Cl$, $[Fe(tpy)_2]Cl_2$ (tpy = 2,2′:6′,2′′-terpyridine), *cis*-$[Fe(cyclen)Cl_2]Cl$ (cyclen = 1,4,7,10-tetraazacyclodecane) and *trans*-$Fe(TMC)Br_2$ (TMC = 1,4,8,11-tetramethyl-1,4,8,11-tetraazacyclotetradecane), can also catalyse WOR by a one-electron oxidant such as $[Ru(bpy)_3]^{3+}$ to evolve O_2 at pH 7 – 9.[286] These Fe(II) complexes can also be used as a WOC for the photocatalytic WOR by $Na_2S_2O_8$ with $[Ru(bpy)_3]^{2+}$ (Scheme 3).[285,286] However, $Fe(ClO_4)_3$ without organic ligands acted as a precursor of a true WOC and afforded the largest O_2 yield (48%), when NPs (500–1200 nm) composed of Fe_2O_3, which was identified by energy-dispersive X-ray spectroscopy and XPS measurements, were observed in DLS measurements.[286] Thus, the true catalysts derived from the Fe(II) complexes with tetradentate N donor ligands in the thermal and photochemical WORs are different depending on the pH of reaction solutions.[285,286] The iron(IV)-oxo species produced as the reactive intermediate for the O-O bond formation in the catalytic WOR is unstable at high pH, where Fe complexes undergo hydrolysis, accompanied by the ligand oxidation to generate Fe_2O_3, which is the true catalyst for the catalytic WOR at high pH.[286]

A Fe^{III} complex of biuretmodified tetra-amidomacrocyclic ligand ($[(bTAML)Fe^{III}]^-$) was also used as a WOC in the photochemical WOR by $Na_2S_2O_8$ with $[Ru(bpy)_3]^{2+}$ (Scheme 3) in pH 8.7 borate buffer to afford TON = 220 ± 10 and ~44% O_2 yield.[287] The higher TON of 900 and O_2 yield of 48% with the quantum yield of 24% were obtained by using an inorganic molecular tetra-iron(III)-substituted polyoxotungstate $[Fe^{III}_4(H_2O)_2(P_2W_{15}O_{56})_2]^{12-}$ in pH 9.0 borate buffer.[286] In both cases, no evidence of iron oxide NPs was observed by DLS or TEM measurements.[287,288] The molecular catalytic mechanism of $[(bTAML)Fe^{III}]^-$ is proposed as shown in Scheme 5,[287] where photoexcitation of $[Ru(bpy)_3]^{2+}$ results in ET from $S_2O_8^{2-}$ to the excited state ($[Ru(bpy)_3]^{2+*}$) to produce $[Ru(bpy)_3]^{3+}$ and $SO_4^{\bullet-}$.[289] Then, ET from $[(bTAML)Fe^{III}]^-$ to $[Ru(bpy)_3]^{3+}$ occurs with H_2O to produce $[(bTAML)Fe^{IV}(OH)]^-$ after the depotonation, accompanied by regeneration of $[Ru(bpy)_3]^{2+}$.[287] Two $[(bTAML)Fe^{IV}(OH)]^-$ molecules are converted to the μ-oxo dimer ($[(bTAML)Fe^{IV}(O)Fe^{IV}(bTAML)]^{2-}$) after removal of H_2O. Although the μ-oxo dimer is not further oxidised by $[Ru(bpy)_3]^{3+}$, it is oxidised by $SO_4^{\bullet-}$ to produce the $Fe^{V}(O)$ species ($[(bTAML)Fe^{V}(O)]^-$).[287] When $[(bTAML)Fe^{III}]^-$ is present, fast comproportionation reaction of $[(bTAML)Fe^{V}(O)]^-$ with $[(bTAML)Fe^{III}]^-$ occurs to produce the μ-oxo dimer ($[(bTAML)Fe^{IV}(O)Fe^{IV}(bTAML)]^{2-}$).[290] Then, the nucleophilic attack of water to the $Fe^{V}(O)$ species occurs to produce the monomeric Fe^{III}-hydroperoxo species ($[(bTAML)Fe^{III}(OOH)]^{2-}$) as the case of the $Ru^{V}(O)$ species in Scheme 1.[287] Although the $Fe^{V}(O)$ species ($[(bTAML)Fe^{V}(O)]^-$) was not detected in water due to the instability, the formation of $[(bTAML)Fe^{V}(O)]^-$ was detected by HRMS and EPR when the photochemical WOR was performed using equimolar amounts of $[(bTAML)Fe^{III}]^-$, $[Ru(bpy)_3]^{2+}$ and $Na_2S_2O_8$ (60 μM each) in CH_3CN-buffer (*v*/*v* 1:1).[287] HRMS revealed two peaks; one for the unreacted Fe^{III} complex (*m*/*z* = 413.08 for $[(bTAML)Fe^{III}]^-$) and the other for the $Fe^{V}(O)$ complex (*m*/*z* = 429.07 for $[(bTAML)Fe^{V}(O)]^-$) within the instrumental error limit, which was shifted to 431.08 when $H_2{}^{18}O$ was used instead of $H_2{}^{16}O$.[287]

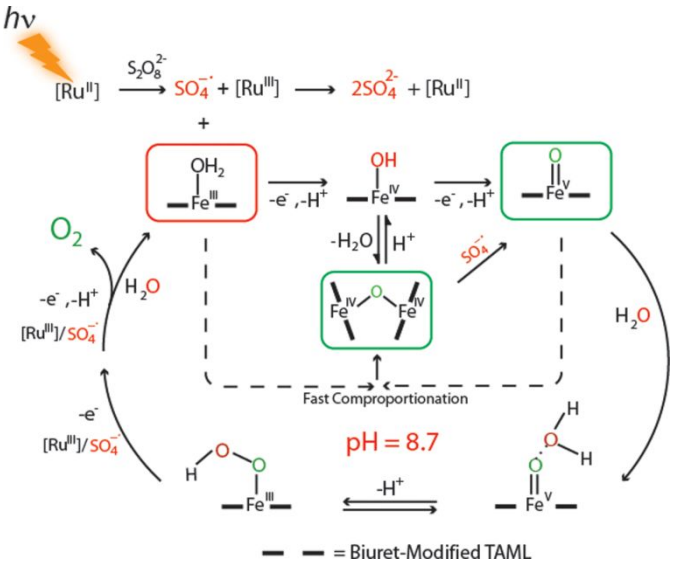

Scheme 5 Proposed mechanism of catalytic photochemical WO by $[(bTAML)Fe^{III}]^-$. Reprinted with permission from reference 287. Copyright 2014, American Chemical Society.

Both $[(TAML)Fe^{III}]^-$ and $[(bTAML)Fe^{III}]^-$ can also catalyse WOR by cerium(IV) ammonium nitrite (CAN) at pH 1 to evolve oxygen with 14% and 4% yields, respectively.[287,291] The low oxygen yields result from the facile demetallation with the strong acid at pH 1.[287,291] The initial oxygen evolution rates were proportional to the concentrations of $[(TAML)Fe^{III}]^-$ and $[(bTAML)Fe^{III}]^-$,[287,291] indicating that the r.d.s. is the nucleophilic attack of water to the $Fe^{V}(O)$ species rather than the radical coupling process.

$[(bTAML)Fe^{III}]^-$ also acts as an efficient catalyst for the electrochemical WOR to evolve O_2 with an overpotential of about 250 mV at pH 7.[292] $[(bTAML)Fe^{III}]^-$ exists as a six-coordinate complex ($[(bTAML)Fe^{III}(H_2O)_2]^-$) with both the water

molecules located at the axial positions of Fe^{III}.[292,293] The pK_a value of the axial H_2O ligands of $([(bTAML)Fe^{III}(H_2O)_2]^-$ in water was determined to be 10.3 by UV-vis titration experiments.[292] The cyclic voltammogram of $[(bTAML)Fe^{III}(H_2O)_2]^-$ exhibited the first oxidation peak potential at 0.85 V *vs*. NHE at pH 7 and the peak potential decreased with increasing pH by 117 mV (pH unit) between pH 7 and 10.[292] This indicates a proton-coupled electron-transfer (PCET) oxidation of $[(bTAML)Fe^{III}(H_2O)_2]^-$ associated with removal of two protons to produce $[(bTAML)Fe^{IV}(O)(H_2O)]^{2-}$ [eqn (6)] as the case of

$$[(bTAML)Fe^{III}(H_2O)_2]^- - e^- \rightarrow [(bTAML)Fe^{IV}(O)(H_2O)]^{2-} + 2H^+ \quad (6)$$

$[(bTAML)Co^{III}]^-$ [eqn (4)].[292] When H_2O was replaced by D_2O, the first irreversible wave was shifted by 80 mV to afford the deuterium kinetic isotope effect (KIE = 3.2).[292] The KIE indicates that the O-H/O-D bond cleavage is involved in the PCET process in eqn (6). The second oxidation peak was observed at 1.25 V vs. NHE at pH 7 with a drastically enhanced current above the background. This oxidation peak potential was pH-independent between pH 7 and 10, corresponding to the one-electron oxidation of $[(bTAML)Fe^{IV}(O)(H_2O)]^{2-}$ to the $Fe^{V}(O)$ species ($[(bTAML)Fe^{V}(O)(H_2O)]^-$) [eqn (7)]. Controlled-potential electrolysis of 1 mM $[(bTAML)Fe^{III}(H_2O)_2]^-$ in pH 7.2 phosphate buffer (15 mm) on 1 cm^2 platinum foil at 1.26 V *vs*. NHE for 2h afforded a total charge of 0.8 C to yield 186 μM of O_2, which corresponds to 89.9% Faradic efficiency.[292] Although the formation of the $Fe^{V}(O)$ species was not detected during the electrolysis in pure water, electrolysis of $[(bTAML)Fe^{III}(H_2O)_2]^-$ in CH_3CN/H_2O (v/v 9:1) at 1.25 V *vs*. NHE for 60 s resulted in the formation of the $Fe^{V}(O)$ species ($[(bTAML)Fe^{V}(O)(H_2O)]^-$), which was detected by the characteristic UV-vis peaks at 445 and 613 nm as well as by HRMS.[292]

$$[(bTAML)Fe^{IV}(O)(H_2O)]^{2-} - e^- \rightarrow [(bTAML)Fe^{V}(O)]^- + H_2O \quad (7)$$

The highest TOF value (1900 s^{-1}) was reported using a pentanuclear iron complex, $[Fe^{II}_4Fe^{III}(\mu_3\text{-}O)(\mu\text{-}L)_6]^{3+}$ (LH = 3,5-bis(2-pyridyl)pyrazole), in an acetonitrile/water (10:1) mixed solution with Et_4NClO_4 (0.10 M).[294] However, the large overpotential (η = 0.5 V) has precluded the practical application.[294] The overpotential was reduced to 340 mV at 10 mA cm^{-2} in 1.0 KOH aqueous solution using Fe-(tetracyanoquinodimethane)$_2$ ($Fe(TCNQ)_2$), that is a conductive MOF to show the long-term electrochemical durability with its catalytic activity being retained for at least 110 h.[295]

4. Mixed Metal Oxide Nanoparticles

As mentioned above, manganese-oxo-calcium clusters (Mn_4CaO_5) catalyse efficiently WOR by the OEC in PSII.[84-93] The Ca^{2+} ion in the OEC is proposed to play the pivotal role to regulate the oxidising reactivity of the $Mn^{V}(O)$ reactive intermediate based on studies on metal ion-coupled electron-transfer (MCET) reactions.[296-302] Inspired by the important role of Ca^{2+} ion, redox-inactive metal ions were introduced to metal oxides to generate mixed metal oxides to enhance the WOR catalytic activity. This naïve idea was tested by using perovskite ($LaCoO_3$, $NdCoO_3$, $YCoO_3$, $La_{0.7}Sr_{0.3}CoO_3$) and wolframite ($CoWO_4$) as WOCs in comparison with spinel (Co_3O_4) for the photochemical WOR by $Na_2S_2O_8$ with $[Ru(bpy)_3]^{2+}$, as shown in Fig. 20.[303]

The decay rates of $[Ru(bpy)_3]^{3+}$ in the WOR with $LaCoO_3$ (brown) and $La_{0.7}Sr_{0.3}CoO_3$ (red) are faster than that without catalyst.[303] The O_2 yields in the photocatalytic WOR by $Na_2S_2O_8$ with $[Ru(bpy)_3]^{2+}$ using $LaCoO_3$, $CoWO_4$, Co_3O_4 and $La_{0.7}Sr_{0.3}CoO_3$ as WOCs at pH 7.0 were 74%, 19%, 59% and 47%, respectively (Fig. 20b).[303] Among cobalt-containing mixed metal oxides, $LaCoO_3$ exhibited the highest WOR catalytic activity.[303]

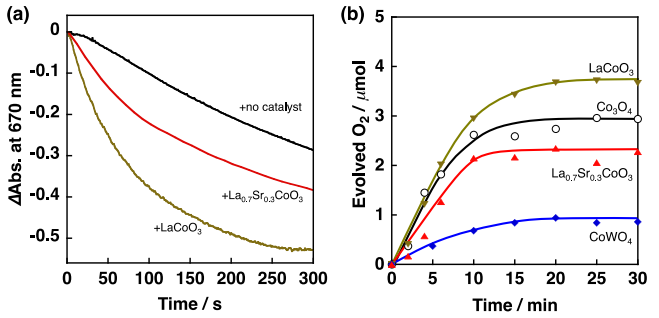

Fig. 20 (a) Decay tile profiles of absorbance at 670 nm due to $[Ru(bpy)_3]^{3+}$ (0.20 mM) in the absence and presence of a cobalt-containing mixed metal oxide WOC (63 mg L^{-1}, black, none; red, $La_{0.7}Sr_{0.3}CoO_3$; brown, $LaCoO_3$) in a phosphate buffer solution (pH 7.0) at 298 K. (b) O_2 evolution time profile of the photocatalytic WOR by $Na_2S_2O_8$ (5.0 mM) with $[Ru(bpy)_3]^{2+}$ (0.25 mM) and a cobalt-containing mixed metal oxide WOC [0.25 g L^{-1}, Co_3O_4 (black), $LaCoO_3$ (brown), $La_{0.7}Sr_{0.3}CoO_3$ (red) and $CoWO_4$ (blue)] under visible light irradiation ($\lambda > 420$ nm) of a phosphate buffer solution (pH 7.0) with a Xe lamp. Reprinted with permission from reference 303. Copyright 2012, Royal Society of Chemistry.

The partial replacement of La^{3+} with Sr^{2+} resulted in the formation of Co^{IV} species in cobalt-containing perovskite, leading to a decrease in the catalytic activity.[303] On the other hand, the replacement of La^{3+} with Nd^{3+} and Y^{3+} resulted in no significant change in the catalytic activity of $NdCoO_3$ and $YCoO_3$ as compared with $LaCoO_3$.[303] Thus, the trivalent metal ions acting as strong Lewis acids enhanced the oxidation activity of Co^{IV} species for the WOR.[303]

The catalytic reactivity for photocatalytic WOR by $Na_2S_2O_8$ with $[Ru(bpy)_3]^{2+}$ was also improved by doping Ni^{2+} ion to iron oxides used as a WOC. Although the catalytic activity of Fe_2O_3 is lower than that of Fe_3O_4 and Co_3O_4 in the photocatalytic WOR as shown in Fig. 21a, $NiFe_2O_4$ NPs exhibited the highest catalytic activity with the largest O_2 yield (74 %) as compared with $MgFe_2O_4$ and $MnFe_2O_4$ NPs (Fig. 21b).[304] Recycle of $NiFe_2O_4$ NPs showed no significant change in the total amount of O_2 evolution in the 2nd and 3rd runs from the reaction solutions, demonstrating that $NiFe_2O_4$ acts as an efficient and robust catalyst for the photocatalytic WOR.[304]

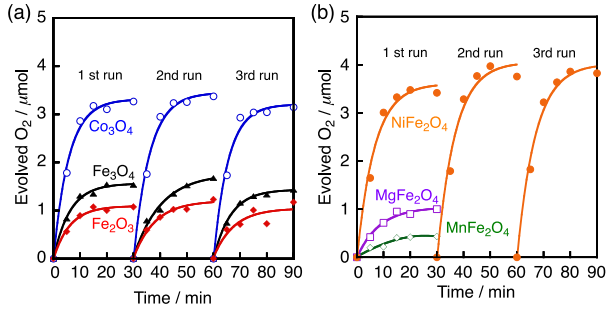

Fig. 21 (a) O_2 evolution time profiles of the photocatalytic WOR by $Na_2S_2O_8$ (5.0 mM) with $[Ru(bpy)_3]^{2+}$ (0.25 mM) and Fe_2O_3, Fe_3O_4 or Co_3O_4 as a WOC (0.50 g L^{-1}) under photoirradiation of a phosphate buffer solution (pH 8.0) with a Xenon lamp ($\lambda > 420$ nm) at room temperature in three recycle examinations. (b) O_2 evolution time profiles with a WOC ($NiFe_2O_4$, $MgFe_2O_4$ or $MnFe_2O_4$) under the same experimental conditions as those of (a). Reprinted with permission from reference 304. Copyright 2012, American Chemical Society.

The $NiFe_2O_4$ NPs/NiFe layered double hydroxide (LDH) nanosheet heterostructure array on Ni foam was reported to display high catalytic activity toward the OER with a very small overpotential of 213 mV at 100 mA cm^{-2},[305] which is smaller than other nanocomposite catalysts.[305-315] Moreover, it also exhibits outstanding HER activity with a very small overpotential of 101 mV at 10 mA cm^{-2}.[305] The $NiFe_2O_4$ NPs/NiFe LDH nanosheet array electrodes also exhibit excellent stability against OER, HER and also the overall water splitting at large current densities. The overall water splitting with $NiFe_2O_4$ NPs/NiFe LDH nanosheets employed as both the anode and the cathode can be continuously driven by a battery of 1.5 V.[305]

The most efficient catalyst for photocatalytic WOR in a buffer solution (pH 7.0) containing $[Ru(bpy)_3]^{2+}$ and $Na_2S_2O_8$ was obtained by incorporation of a small amount of Ca^{2+} ions into a polymeric cobalt cyanide complex to form $Ca_x[Co^{II}(H_2O)_2]_{1.5-x}[Co^{III}(CN)_6]$ (**27** in Fig. 22).[316] The maximum quantum efficiency of 200 % was achieved by using $[Ca_{0.06}[Co^{II}(H_2O)_2]_{1.44}[Co^{III}(CN)_6]$ as a WOC when one photon absorption of $[Ru(bpy)_3]^{2+}$ with $Na_2S_2O_8$ results in generation of two molecules of $[Ru(bpy)_3]^{3+}$ (Scheme 3).[316]

The lowest overpotential of 65 mV at 10 mA cm^{-2} for WOR was achieved by using binary Ni–Fe sulphides supported on nickel foam (NF) used as a WOC in 0.10 M KOH.[317] However, the NiFeS/NF catalyst was not stable due to the intrinsic nature of metal sulphides in alkaline solution.[317] Electrodeposition of Fe hydroxide film on NiFeS/NF(NiFeS–Fe/NF) has been performed to protect NiFeS/NF for better stability during electrocatalytic WOR. The enhanced stability was compensated by the lower activity with higher overpotential of 101.6 mV at 10 mA cm^{-2}.[317]

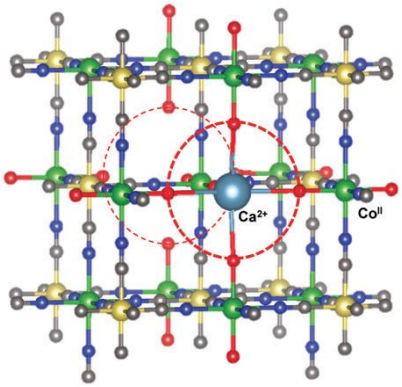

Fig. 22 A drawing of $Ca_x[Co^{II}(H_2O)_2]_{1.5-x}[Co^{III}(CN)_6]$ (**27**). Elements are colour-coded: Co^{III} (yellow), C (gray), N (blue), CoII (green), O (red), and Ca (cyan). Reprinted with permission from reference 316. Copyright 2017, Royal Society of Chemistry.

5. Conclusions

Whether WOCs are homogeneous or heterogeneous is determined by metals, supporting ligands, pH, oxidants and even concentrations of WOCs. A mononuclear ruthenium polyoxometalate complex (RuPOM) acts as a homogeneous WOC for WOR by CAN because the inorganic POM ligand is difficult to be oxidised during the catalytic WOR. The kinetic analysis together with the detection of the $Ru^{V}(O)$ intermediates indicates that the r.d.s. of the catalytic WOR is the nucleophilic attack of water to the $Ru^{V}(O)$ intermediate. In contrast, organic ligands of Ir(III) complexes were oxidised during the WOR by CAN, leading to the formation of $Ir(OH)_3$ NPs with organic residues, which act as a true WOC. The organic ligands of Co(III) complexes were also oxidised in the photocatalytic WOR by $Na_2S_2O_8$ with $[Ru(bpy)_3]^{2+}$ at pH 7 – 8 to produce $Co(OH)_x$ NPs acting as an actual WOC. MnO_x NPs were also produced via the oxidation of organic ligands of Mn complexes during the catalytic WOR by CAN, acting as a much more active WOC than the precursors. In contrast, some Fe(II) complexes act as homogeneous WOCs in the catalytic WOR by CAN, although the catalyst lifetime was short due to the demetallation reaction under acidic conditions. Under alkaline conditions, however, the Fe(II) complexes act as precursors for the photocatalytic WOR by $Na_2S_2O_8$ with $[Ru(bpy)_3]^{2+}$, where iron oxide NPs were produced to act as a true WOC. Bioinspired by the pivotal role of Ca^{2+} in the OEC in PSII, mixed metal oxide NPs composed of redox-active metal ions and redox-inactive metal ions have been developed as efficient WOCs. The highest catalytic activity for photocatalytic WOR by $Na_2S_2O_8$ was achieved by incorporation of a small amount of Ca^{2+} ions into a polymeric cobalt cyanide complex to form $Ca_x[Co^{II}(H_2O)_2]_{1.5-x}[Co^{III}(CN)_6]$ (Fig. 22). The interdisciplinary approach between the homogeneous and heterogeneous WOCs will enhance the research progress towards clarification of the catalytic mechanism and intermediates as well as practical applications of WOCs in order to meet the rapidly growing demand for the development of sustainable solar fuels via WORs.

Acknowledgements

The authors gratefully acknowledge the contributions of their collaborators and co-workers in the cited references, and the financial supports by a JSPS grant (Grant Number 16H02268 to S.F.) from MEXT, a SENTAN project from JST, the NRF of Korea through CRI (NRF-2012R1A3A2048842 to W.N), GRL (NRF-2010-00353 to W.N.) and Basic Science Research Program (2017R1D1A1B03029982 to Y.M.L. and 2017R1D1A1B03032615 to S.F.).

Notes and references

1 D. Lips, J. M. Schuurmans, F. Branco dos Santos and K. J. Hellingwer, *Energy Environ. Sci.*, 2018, **11**, 10-22.
2 Nathan S. Lewis, *Nat. Nanotechnol*., **2016**, *11*, 1010-1019.
3 T. A. Faunce, W. Lubitz, A. W. Rutherford, D. MacFarlane, G. F. Moore, P. Yang, D. G. Nocera, T. A. Moore, D. H. Gregory, S. Fukuzumi, K. B. Yoon, F. A. Armstrong, M. R. Wasielewski and S. Styring, *Energy Environ. Sci*., 2013, **6**, 695-698.
4 H. B. Gray, *Nat. Chem*., 2009, **1**, 7.
5 D. L. Royer, R. A. Berner and J. Park, *Nature*, 2007, **446**, 530-532.
6 N. S. Lewis and D. G. Nocera, *Proc. Natl. Acad. Sci., USA*, 2006, **103**, 15729-15735.
7 S. Fukuzumi, *Joule*, 2017, **1**, 689-738.
8 S. Fukuzumi, Y.-M. Lee and Wonwoo Nam, *ChemPhotoChem*, 2018, **10**, 9-28.
9 S. J. Mora, E. Odella, G. F. Moore, D. Gust, T. A. Moore and A. L. Moore, *Acc. Chem. Res*., 2018, **51**, 445-453.
10 S. Fukuzumi, Y.-M. Lee and Wonwoo Nam, *Chem.–Eur. J*., **2018**, *24*, 5016-5031.
11 M. E. El-Khouly, E. El-Mohsnawy and S. Fukuzumi, *J. Photochem. Photobiol. C: Photochem. Rev*., 2017, **31**, 36-83.
12 P. Sharma and M. L. Kolhe, *Int. J. Hydrogen Energy*, 2017, **42**, 22704-22712.
13 C. Jiang, S. J. A. Moniz, A. Wang, T. Zhang and J. Tang, *Chem. Soc. Rev*., 2017, **46**, 4645-4660.
14 K. K. Sakimoto, N. Kornienko and P. Yang, *Acc. Chem. Res*., 2017, **50,** 476-481.
15 L. Hammarström, *Faraday Discuss*., 2017, **198**, 549-560.
16 H. Dau, E. Fujita and L. Sun, *ChemSusChem*, 2017, **10**, 4228-4235.
17 J. Su and L. Vayssieres, *ACS Energy Lett*., 2016, **1**, 121-135.
18 W. Kim, E. Edri and H. Frei, *Acc. Chem. Res*., 2016, **49**, 1634-1645.
19 N. Armaroli and V. Balzani, *Chem.–Eur. J*., 2016, **22**, 32-57.
20 D. Bae, B. Seger, P. C. K. Vesborg, O. Hansen and I. Chorkendorff, *Chem. Soc. Rev*., 2017, **46**, 1933-1954.
21 W.-J. Ong, L.-L. Tan, Y. H. Ng, S.-T. Yong and S.-P. Chai, *Chem. Rev*., 2016, **116**, 7159-7329.
22 L. Hammarström, *Acc. Chem. Res*., 2015, **48**, 840-850
23 T. Hisatomi, J. Kubota and K. Domen, *Chem. Soc. Rev*., 2014, **43**, 7520-7535.
24 D. G. Nocera, *Acc. Chem. Res*., 2012, **45**, 767-776
25 K. Maeda and K. Domen, *J. Phys. Chem. Lett*., 2010, **1**, 2655-2661.
26 A. Kudo and Y. Miseki, *Chem. Soc. Rev*., 2009, **38**, 253-278.
27 M. J. Llansola-Portoles, D. Gust, T. A. Moore and A. L. Moore, *C. R. Chimie*, 2017, **20**, 296-313.
28 S. Fukuzumi*, ECS J. Solid State Sci. Technol*., 2017, **6**, M3055-M3061.
29 M. Rudolf, S. V. Kirner and D. M. Guldi, *Chem. Soc. Rev*., 2016, **45**, 612-630.
30 C. B. KC and F. D'Souza, *Coord. Chem. Rev*., 2016, **322**, 104-141.
31 S. Fukuzumi, K. Ohkubo and T. Suenobu, *Acc. Chem. Res*., 2014, **47**, 1455−1464.
32 S. Fukuzumi and K. Ohkubo, *Dalton Trans.*, 2013, **42**, 15846-15858.
33 S. Fukuzumi and K. Ohkubo, *J. Mater. Chem*., 2012, **22**, 4575-4587.
34 D. Gust, T. A. Moore and A. L. Moore, *Acc. Chem. Res*., 2009, **42**, 1890-1898.
35 S. Fukuzumi and T. Kojima, *J. Mater. Chem*., 2008, **18**, 1427-1439.
36 S. Fukuzumi, *Eur. J. Inorg. Chem*., 2008, **2008**, 1351-1362.
37 V. Balzani, A. Credi and M. Venturi, *ChemSusChem*, 2008, **1**, 26-58.
38 S. Fukuzumi, *Phys. Chem. Chem. Phys*., 2008, **10**, 2283-2297.
39 M. R. Wasielewski, *Acc. Chem. Res*., **2009**, *42*, 1910-1921.
40 P. D. Frischmann, K. Mahata and F. Würthner, *Chem. Soc. Rev*., 2013, **42**, 1847-1870.
41 D. Gust, T. A. Moore and A. L. Moore, *Acc. Chem. Res*., 2001, **34**, 40-48.
42 M. N. Paddon-Row, *Adv. Phys. Org. Chem*., 2003, **38**, 1-85.
43 M. R. Wasielewski, *Chem. Rev.*, 1992, **92**, 435-461.
44 M. Rudolf, S. Wolfrum, D. M. Guldi, L. Feng, T. Tsuchiya, T. Akasaka and L. Echegoyen, *Chem.–Eur. J*., 2012, **18**, 5136-5148.
45 D. M. Guldi, G. M. A. Rahman, V. Sgobba and C. Ehli, *Chem. Soc. Rev*., 2006, **35**, 471-487.
46 G. Bottari, G. de la Torre, D. M. Guldi and T. Torres, *Chem. Rev*., 2010, **110**, 6768-6816.
47 S. Fukuzumi, *Bull. Chem. Soc. Jpn.*, 2006, **79**, 177-195.
48 F. D'Souza and O. Ito, *Chem. Soc. Rev*., 2012, **41**, 86-96.
49 F. D'Souza and O. Ito, *Chem. Commun*., 2009, 4913-4928.
50 R. Chitta, F. D'Souza, *J. Mater. Chem*., 2008, **18**, 1440-1471.
51 S. Fukuzumi, Y.-M. Lee and W. Nam, *Coord. Chem. Rev*., 2018, **355**, 54-73.
52 P.-Q. Liao, J.-Q. Shen and J.-P. Zhang, *Coord. Chem. Rev*., 2018, **373**, 22-48.
53 Q. Li and S. Sun, *Nano Energy*, 2016, **29**, 178-197.
54 H. Song, *Acc. Chem. Res*., 2015, **48**, 491-499.
55 S. Fukuzumi, Y. Yamada, T. Suenobu, K. Ohkubo and H. Kotani, *Energy Environ. Sci*., 2011, **4**, 2754-2766.
56 S. Fukuzumi, *Curr. Opin. Chem. Biol*., **2015**, *25*, 18-26.
57 J. D. Benck, T. R. Hellstern, J. Kibsgaard, P. Chakthranont and T. F. Jaramillo, *ACS Catal*., 2014, **4**, 3957-3971.
58 H. Kotani, R. Hanazaki, K. Ohkubo, Y. Yamada and S. Fukuzumi, *Chem.–Eur. J.*, 2011, **17**, 2777-2785.
59 Y. Yamada, T. Miyahigashi, H. Kotani, K. Ohkubo and S. Fukuzumi, *J. Am. Chem. Soc.*, 2011, **133,** 16136-16145.
60 Y. Yamada, T. Miyahigashi, H. Kotani, K. Ohkubo and S. Fukuzumi, *Energy Environ. Sci.*, 2012, **5**, 6111-6118.
61 B. Mondal, K. Sengupta, A. Rana, A. Mahammed, M. Botoshansky, S. G. Dey, Z. Gross and A. Dey, *Inorg. Chem*., 2013, **52**, 3381−3387.
62 M. J. Rose, H. B. Gray and J. R. Winkler, *J. Am. Chem. Soc.*, 2012, **134**, 8310−8313.
63 T. M. McCormick, Z. Han, D. J. Weinberg, W. W. Brennessel, P. L. Holland and R. Eisenberg, *Inorg. Chem*., 2011, **50**, 10660-10666.
64 Z. Han, W. R. McNamara, M. S. Eum, P. L. Holland and R. Eisenberg, *Angew. Chem., Int. Ed*., 2012, **51**, 1667-1670.

65 H. I. Karunadasa, C. J. Chang and J. R. Long, *Nature*, 2010, **464**, 1329-1333.
66 H. I. Karunadasa, E. Montalvo, Y. Sun, M. Majda, J. R. Long and C. J. Chang, *Science*, 2012, **335**, 698-702.
67 A. E. King, Y. Surendranath, N. A. Piro, J. P. Bigi, J. R. Long and C. J. Chang, *Chem. Sci*., 2013, **4**, 1578-1587.
68 V. S. Thoi, Y. Sun, J. R. Long and C. J. Chang, *Chem. Soc. Rev*., 2013, **42**, 2388-2400.
69 E. J. Sundstrom, X. Yang, V. S. Thoi, H. I. Karunadasa, C. J. Chang, J. R. Long and M. Head-Gordon, *J. Am. Chem. Soc*., 2012, **134**, 5233-5242.
70 Y. Sun, J. P. Bigi, N. A. Piro, M. L. Tang, J. R. Long and C. J. Chang, *J. Am. Chem. Soc*., 2011, **133**, 9212-9215.
71 X. Li, Mei Wang, D. Zheng, K. Han, J. Donga and L. Sun, *Energy Environ. Sci*., 2012, **5**, 8220-8224.
72 L. Chen, M. Wang, F. Gloaguen, D. Zheng, P. Zhang and L. Sun, *Inorg. Chem*., 2013, **52**, 1798-1806.
73 J. Dong, M. Wang, X. Li, L. Chen, Y. He and L. Sun, *ChemSusChem*, 2012, **5**, 2133-2138.
74 N. Onishi, C. Laurenczy, M. Beller and Y. Himeda, *Coord. Chem. Rev*., 2018, **373**, 317-332.
75 J. Artz, T. E. Müller and K. Thenert, *Chem. Rev*., 2018, **118**, 434-504.
76 A. Glüer and S. Schneider, *J. Organomet. Chem*., 2018, **861**, 159-173.
77 K. A. Grice, *Coord. Chem. Rev*., 2017, **336**, 78-95.
78 W.-H. Wang, Y. Himeda, J. T. Muckerman, G. F. Manbeck and E. Fujita, *Chem. Rev*., 2015, **115**, 12936-12973.
79 S. Fukuzumi and T. Suenobu, *Dalton Trans*., 2013, **42**, 18-28.
80 Y. Maenaka, T. Suenobu and S. Fukuzumi, *Energy Environ. Sci*., 2012, **5**, 7360-7367.
81 E. Fujita, J. T. Muckerman and Y. Himeda, *Biochim. Biophys. Acta*, 2013, **1827**, 1031-1038.
82 W.-H. Wang, J. F. Hull, J. T. Muckerman, E. Fujita and Y. Himeda, *Energy Environ. Sci*., 2012, **5**, 7923-7926.
83 J. F. Hull, Y. Himeda, W.-H. Wang, B. Hashiguchi, R. Periana, D. J. Szalda, J. T. Muckerman and E. Fujita, *Nat. Chem*., 2012, **4**, 383-388.
84 M. M. Najafpour, S. Heidari, S. E. Balaghi, M. Hołyńska, M. H. Sadr, B. Soltani, M. Khatamian, A. W. Larkum and S. I. Allakhverdiev, *Biochim. Biophys. Acta*, 2017, **1858**, 156-174.
85 M. Suga, F. Akita, M. Sugahara, M. Kubo, Y. Nakajima, T. Nakane, K. Yamashita, Y. Umena, M. Nakabayashi, T. Yamane, T. Nakano, M. Suzuki, T. Masuda, S. Inoue, T. Kimura, T. Nomura, S. Yonekura, L.-J. Yu, T. Sakamoto, T. Motomura, J.-H. Chen, Y. Kato, T. Noguchi, K. Tono, Y. Joti, T. Kameshima, T. Hatsui, E. Nango, R. Tanaka, H. Naitow, Y. Matsuura, A. Yamashita, M. Yamamoto, O. Nureki, M. Yabashi, T. Ishikawa, S. Iwata and J.-R. Shen, *Nature*, 2017, **543**, 131-135.
86 M. Askerka, G. W. Brudvig and V. S. Batista, *Acc. Chem. Res*., 2017, **50**, 41-48.
87 J. Barber, *Biochemistry*, 2016, **55**, 5901-5906.
88 J.-R. Shen, *Ann. Rev. Plant Biol*., 2015, **66**, 23-48.
89 D. J. Vinyard, S. Khan and G. W. Brudvig, *Faraday Discuss*., 2015, **185**, 37-50.
90 M. M. Najafpour, M. A. Isaloo, J. J. Eaton-Rye, T. Tomo, H. Nishihara, K. Satoh, R. Carpentier, J.-R. Shen and S. I. Allakhverdiev, *Biochim. Biophys. Acta*, 2014, **1837**, 1395-1410.
91 N. Cox, M. Retegan, F. Neese, D. A. Pantazis, A. Boussac and W. Lubitz, *Science*, 2014, **345**, 804-808
92 N. Cox, D. A. Pantazis, F. Neese and W. Lubitz, *Acc. Chem. Res*., 2013, **46**, 1588-1596.
93 Y. Umena, K. Kawakami, J.-R. Shen and N. Kamiya, *Nature*, 2011, **473**, 55-60.
94 W. Zhang, W. Lai and R. Cao, *Chem. Rev*., 2017, **117**, 3717-3797.
95 T. K. Michaelos, D. Y. Shopov, S. B. Sinha, L. S. Sharninghausen, K. J. Fisher, H. M. C. Lant, R. H. Crabtree and G. W. Brudvig, *Acc. Chem. Res*., 2017, **50**, 952-959.
96 S. Fukuzumi, T. Kojima, Y.-M. Lee and W. Nam, *Coord. Chem. Rev*., 2017, **333**, 44-56.
97 D. G. H. Hetterscheid, *Chem. Commun*., 2017, **53**, 10622-10631.
98 D. W. Shaffer, Y. Xie and J. J. Concepcion, *Chem. Soc. Rev*., 2017, **46**, 6170-6193.
99 T. J. Meyer, M. V. Sheridan and B. D. Sherman, *Chem. Soc. Rev*., 2017, **46**, 6148-6169.
100 P. Garrido-Barros, C. Gimbert-Suriñach, R. Matheu, X. Sala and A. Llobet, *Chem. Soc. Rev*., 2017, **46**, 6088-6098.
101 M. D. Kärkäs and B. Åkermark, *Dalton Trans*., 2016, **45**, 14421-14461.
102 J. D. Blakemore, R. H. Crabtree and G. W. Brudvig, *Chem. Rev*., 2015, **115**, 12974-13005.
103 L. Duan, L. Wang, F. Li, F. Li and L. Sun, *Acc. Chem. Res*., 2015, **48**, 2084−2096.
104 Q. Zeng, F. W. Lewis, L. M. Harwood and F. Hartl, *Coord. Chem. Rev*., 2015, **304**-**305**, 88-101.
105 X. Sala, S. Maji, R. Bofill, J. García-Antón, L. Escriche and A. Llobet, *Acc. Chem. Res*., 2014, **47**, 504-516.
106 A. R. Parent and K. Sakai, *ChemSusChem*, 2014, **7**, 2070-2080.
107 X. Liu, F. Wang, *Coord. Chem. Rev*., 2012, **256**, 1115-1136.
108 M. Natali, I. Bazzan, S. Goberna-Ferrón, R. Al-Oweini, M. Ibrahim, B. S. Bassil, H. Dau, F. Scandola, J. R. Galán-Mascarós, U. Kortz, A. Sartorel, I. Zaharieva and M. Bonchio, *Green Chem*., 2017, **19**, 2416-2426.
109 B. M. Hunter, H. B. Gray and A. M. Müller, *Chem. Rev*., 2016, **116**, 14120-14136.
110 D. Chen, C. Chen, Z. M. Baiyee, Z. Shao and F. Ciucci, *Chem. Rev*., 2015, **115**, 9869-9921.
111 S. Fukuzumi and Y. Yamada, *J. Mater. Chem*., 2012, **22**, 24284-24296.
112 F. Jiao and H. Frei, *Angew. Chem., Int. Ed*., 2009, **48**, 1841-1844.
113 F. Jiao and H. Frei, *Energy Environ. Sci*., 2010, **3**, 1018-1027.
114 Q. Zhao, Z. Yan, C. Chen and J. Chen, *Chem. Rev*., 2017, **117**, 10121-10211.
115 N.-T. Suen, S.-F. Hung, Q. Quan, N. Zhang, Y.-J. Xu and H. M. Chen, *Chem. Soc. Rev*., 2017, **46**, 337-365.
116 J. R. Galán-Mascarós, *ChemElectroChem*, 2015, **2**, 37-50.
117 E. Fabbri, A. Habereder, K. Waltar, R. Kötz and T. J. Schmidt, *Catal. Sci. Technol*., 2014, **4**, 3800-3821.
118 K. Jin, H. Seo, H. Ha, Y. Kim, K. H. Cho, J. S. Hong and K. T. Nam, *Catal. Today*, 2018, DOI: 10.1016/j.cattod.2016.12.041.
119 C. H. M. van Oversteeg, H. Q. Doan, F. M. F. de Groot and T. Cuk, *Chem. Soc. Rev*., 2017, **46**, 102-125.

120 T. Zhang, Y. Zhu and J. Y. Lee, *J. Mater. Chem. A*, 2018, **6**, 8147-8158.
121 A. Indra, P. W. Menezes and M. Driess*, ChemSusChem*, 2015, **8**, 776-785.
122 J. Hessels, R. J. Detz, M. T. M. Koper and J. N. H. Reek, *Chem.–Eur. J*., 2017, **23**, 16413-16418.
123 A. Sartorel, M. Bonchio, S. Campagnab and F. Scandola, *Chem. Soc. Rev*., 2013, **42**, 2262-2280.
124 C. J. Gagliardi, A. K. Vannucci, J. J. Concepcion, Z. Chen and T. J. Meyer, *Energy Environ. Sci*., 2012, **5**, 7704-7717.
125 D. G. H. Hetterscheid and J. N. H. Reek, *Angew. Chem., Int. Ed*., 2012, **51**, 9740-9747.
126 K. S. Joya, J. L. Vallés-Pardo, Y. F. Joya, T. Eisenmayer, B. Thomas, F. Buda and H. J. M. de Groot, *ChemPlusChem*, 2013, **78**, 35-47.
127 F. Puntoriero, A. Sartorel, M. Orlandic, G. La Ganga, S. Serronia, M. Bonchio, F. Scandola and S. Campagn, *Coord. Chem. Rev*., 2011, **255**, 2594-2601.
128 H. Lv, Y. V. Geletii, C. Zhao, J. W. Vickers, G. Zhu, Z. Luo, J. Song, T. Lian, D. G. Musaevb and C. L. Hill, *Chem. Soc. Rev*., 2012, **41**, 7572-7589.
129 A. R. Parent, R. H. Crabtree and G. W. Brudvig, *Chem. Soc. Rev*., 2013, **42**, 2247-2252.
130 D. J. Wasylenko, R. D. Palmer and C. P. Berli, *Chem. Commun*., 2013, **49**, 218-227.
131 R. Cao, W. Laia and P. Du, *Energy Environ. Sci*., 2012, **5**, 8134-8157.
132 V. Artero and M. Fontecave, *Chem. Soc. Rev*., 2013, **42**, 2338-2356.
133 R. H. Crabtree, *Chem. Rev*., 2012, **112**, 1536-1554.
134 S. W. Gersten, G. J. Samuels and T. J. Meyer, *J. Am. Chem. Soc*., 1982, **104**, 4029−4030.
135 D. Moonshiram, J. W. Jurss, J. J. Concepcion, T. Zakharova, I. Alperovich, T. J. Meyer and Y. Pushkar, *J. Am. Chem. Soc*., 2012, **134**, 4625-4636.
136 M. R. Norris, J. J. Concepcion, D. P. Harrison, R. A. Binstead, D. L. Ashford, Z. Fang, J. L. Templeton and T. J. Meyer, *J. Am. Chem. Soc*., 2013, **135**, 2080-2083.
137 D. Moonshiram, I. Alperovich, J. J. Concepcion, T. J. Meyer and Y. Pushkar, *Proc. Natl. Acad. Sci. USA*, 2013, **110**, 3765-3770.
138 L. Duan, A. Fischer, Y. Xu and L. Sun, *J. Am. Chem. Soc*., 2009, **131**, 10397-10399.
139 L. Francás, X. Sala, E. Escudero-Adán, J. Benet-Buchholz, L. Escriche and A. Llobet, *Inorg. Chem*., 2011, **50**, 2771-2781.
140 Y. Jiang, F. Li, B. Zhang, X. Li, X. Wang, F. Huang and L. Sun, *Angew. Chem., Int. Ed*., 2013, **52**, 3398-3401.
141 R. Zong and R. P. Thummel, *J. Am. Chem. Soc*., 2005, **127**, 12802-12803.
142 J. J. Concepcion, J. W. Jurss, J. L. Templeton and T. J. Meyer, *J. Am. Chem. Soc*., 2008, **130**, 16462-16463.
143 J. J. Concepcion, M.-K. Tsai, J. T. Muckerman and T. J. Meyer, *J. Am. Chem. Soc*., 2010, **132**, 1545-1557.
144 D. E. Polyansky, J. T. Muckerman, J. Rochford, R. Zong, R. P. Thummel and E. Fujita, *J. Am. Chem. Soc*., 2011, **133**, 14649-14665.
145 B. Radaram, J. A. Ivie, W. M. Singh, R. M. Grudzien, J. H. Reibenspies, C. Edwin Webster and X. Zhao, *Inorg. Chem*., 2011, **50**, 10564-10571.
146 S. Maji, I. López, F. Bozoglian, J. Benet-Buchholz and A. Llobet, *Inorg. Chem*., 2013, **52**, 3591-3593.
147 J. A. Stull, T. A. Stich, J. K. Hurst and R. D. Britt, *Inorg. Chem*., 2013, **52**, 4578-4586.
148 L. Duana, C. M. Araujob, M. S. G. Ahlquistb and L. Sun, *Proc. Natl. Acad. Sci. U.S.A.*, 2012, **109**, 15584-15588.
149 L. Tong, A. K. Inge, L. Duan, L. Wang, X. Zou and L. Sun, *Inorg. Chem*., 2013, **52**, 2505-2518.
150 L. Tong, M. Göthelid and L. Sun, *Chem. Commun*., 2012, **48**, 10025-10027.
151 Y. V. Geletii, B. Botar, P. Kögerler, D. A. Hillesheim, D. G. Musaev and C. L. Hill, *Angew. Chem., Int. Ed*., 2008, **47**, 3896-3899.
152 Y. V. Geletii, C. Besson, Y. Hou, Q. S. Yin, D. G. Musaev, D. Quinonero, R. Cao, K. I. Hardcastle, A. Proust, P. Kogerler and C. L. Hill, *J. Am. Chem. Soc.*, 2009, **131**, 17360-17370.
153 A. Sartorel, M. Carraro, G. Scorrano, R. D. Zorzi, S. Geremia, N. D. McDaniel, S. Bernhard and M. Bonchio, *J. Am. Chem. Soc*., 2008, **130**, 5006-5007.
154 M. Natali, M. Orlandi, S. Berardi, S. Campagna, M. Bonchio, A. Sartorel and F. Scandola, *Inorg. Chem*., 2012, **51**, 7324-7331.
155 M. Murakami, D. Hong, T. Suenobu and S. Fukuzumi, *J. Am. Chem. Soc*., 2011, **133**, 11605-11613.
156 N. Song, J. J. Concepcion, R. A. Binstead, J. A. Rudd, A. K. Vannucci, C. J. Dares, M. K. Coggins and T. J. Meyer, *Proc. Natl. Acad. Sci. U.S.A*., 2015, **112**, 4935-4940.
157 F. Cai, W. Su, H. A. Younus, K. Zhou, C. Chen, S. Chaemchuen and F. Verpoort, *New. J. Chem*., 2018, **42**, 2476-2482.
158 R. Matheu, M. Z. Ertem, J. Benet-Buchholz, E. Coronado, V. S. Batista, X. Sala and Antoni Llobet, *J. Am. Chem. Soc*., 2015, **137**, 10786-10795.
159 D. Lebedev, Y. Pineda-Galvan, Y. Tokimaru, A. Fedorov, N. Kaeffer, C. Copéret and Y. Pushkar, *J. Am. Chem. Soc*., 2018, **140**, 451-458.
160 Y. Xie, D. W. Shaffer and J. J. Concepcion, *Inorg. Chem*., 2018, **57**, 10533-10542.
161 L. Wang, L. Duan, B. Stewart, M. Pu, J. Liu, T. Privalov and L. Sun, *J. Am. Chem. Soc.*, 2012, **134**, 18868-18880.
162 L. Duan, F. Bozoglian, S. Mandal, B. Stewart, T. Privalov, A. Llobet and L. Sun, *Nat. Chem*., 2012, **4**, 418-423.
163 Q. Daniel, L. Wang, L. Duan, F. Li and L. Sun, *Dalton Trans*., 2016, **45**, 14689-14696.
164 D. W. Shaffer, Y. Xie, D. J. Szalda and J. J. Concepcion, *Inorg. Chem*., 2016, **55**, 12024-12035.
165 R. Matheu, M. Z. Ertem, M. Pipelier, J. Lebreton, D. Dubreuil, J. Benet-Buchholz, X. Sala, A. Tessier and A. Llobet, *ACS Catal*., 2018, **8**, 2039-2048.
166 L.-Å. Näslund, C. M. Sánchez-Sánchez, Á. S. Ingason, J. Bäckström, E. Herrero, J. Rosen and S. Holmin, *J. Phys. Chem. C*, 2013, **117**, 6126-6135.
167 Y. Lee, J. Suntivich, K. J. May, E. E. Perry and Y. Shao-Horn, *J. Phys. Chem. Lett*., 2012, **3**, 399-404.
168 E. Tsuji, A. Imanishi, K. Fukui and Y. Nakato, *Electrochim. Acta*, 2011, **56**, 2009-2016.
169 T. Reier, M. Oezaslan and P. Strasser, *ACS Catal*., 2012, **2**, 1765-1772.
170 I. Jang, I. Hwang and Y. Tak, *Electrochim. Acta*, 2013, **90**, 148-156.

171 W. Hu, Y. Wang, X. Hu, Y. Zhoua and S. Chen, *J. Mater. Chem*., 2012, **22**, 6010-6016.
172 L. Trotochaud, J. K. Ranney, K. N. Williams and S. W. Boettcher, *J. Am. Chem. Soc*., 2012, **134**, 17253-17261.
173 M. E. G. Lyons and S. Floquet, *Phys. Chem. Chem. Phys*., 2011, **13**, 5314-5335.
174 M.-C. Chuang and J. A. Ho, *RSC Adv*., 2012, **2**, 4092-4096.
175 N. Sivasankar, W. W. Weare and H. Frei, *J. Am. Chem. Soc*., 2011, **133**, 12976-12979.
176 J. F. Hull, D. Balcells, J. D. Blakemore, C. D. Incarvito, O. Eisenstein, G. W. Brudvig and R. H. Crabtree, *J. Am. Chem. Soc.*, 2009, **131**, 8730-8731.
177 J. D. Blakemore, N. D. Schley, D. Balcells, J. F. Hull, G. W. Olack, C. D. Incarvito, O. Eisenstein, G. W. Brudvig and R. H. Crabtree, *J. Am. Chem. Soc.*, 2010, **132**, 16017-16029.
178 R. Lalrempuia, N. D. McDaniel, H. Muller-Bunz, S. Bernhard and M. Albrecht, *Angew. Chem., Int. Ed.*, 2010, **49**, 9765-9768.
179 A. Savini, G. Bellachioma, G. Ciancaleoni, C. Zuccaccia, D. Zuccaccia and A. Macchioni, *Chem. Commun.*, 2010, **46**, 9218-9219.
180 D. G. H. Hetterscheid and J. N. H. Reek, *Chem. Commun.*, 2011, **47**, 2712-2714.
181 A. Bucci, A. Savini, L. Rocchigiani, C. Zuccaccia, S. Rizzato, A. Albinati, A. Llobet and A. Macchioni, *Organometallics*, 2012, **31**, 8071-8074.
182 C. Wang, J.-L. Wang and W. Lin, *J. Am. Chem. Soc*., 2012, **134**, 19895-19908.
183 J. DePasquale, I. Nieto, L. E. Reuther, C. J. Herbst-Gervasoni, J. J. Paul, V. Mochalin, M. Zeller, C. M. Thomas, A. W. Addison and E. T. Papish, *Inorg. Chem*., 2013, **52**, 9175-9183.
184 K. S. Joya, N. K. Subbaiyan, F. D'Souza and H. J. M. de Groot, *Angew. Chem., Int. Ed*., 2012, **51**, 9601-9605.
185 W. I. Dzik, S. E. Calvo, J. N. H. Reek, M. Lutz, M. A. Ciriano, C. Tejel, D. G. H. Hetterscheid and B. de Bruin, *Organometallics*, 2011, **30**, 372-374.
186 J. D. Blakemore, M. W. Mara, M. N. Kushner-Lenhoff, N. D. Schley, S. J. Konezny, I. Rivalta, C. F. A. Negre, R. C. Snoeberger, O. Kokhan, J. Huang, A. Stickrath, L. A. Tran, M. L. Parr, L. X. Chen, D. M. Tiede, V. S. Batista, R. H. Crabtree and G. W. Brudvig, *Inorg. Chem*., 2013, **52**, 1860-1871.
187 J. D. Blakemore, N. D. Schley, G. W. Olack, C. D. Incarvito, G. W. Brudvig and R. H. Crabtree, *Chem. Sci*., 2011, **2**, 94-98.
188 M. N. Kushner-Lenhoff, J. D. Blakemore, N. D. Schley, R. H. Crabtree and G. W. Brudvig, *Dalton Trans*., 2013, **42**, 3617-3622.
189 J. D. Blakemore, N. D. Schley, M. N. Kushner-Lenhoff, A. M. Winter, F. D'Souza, R. H. Crabtree and G. W. Brudvig, *Inorg. Chem*., 2012, **51**, 7749-7763.
190 N. D. Schley, J. D. Blakemore, N. K. Subbaiyan, C. D. Incarvito, F. D'Souza, R. H. Crabtree and G. W. Brudvig, *J. Am. Chem. Soc.*, 2011, **133**, 10473-10481.
191 D. Hong, M. Murakami, Y. Yamada and S. Fukuzumi, *Energy Environ. Sci.*, 2012, **5**, 5708-5716.
192 J. Yang, H. Liu, W. N. Martens and R. L. Frost, *J. Phys. Chem. C*, 2010, **114**, 111-119.
193 Y. Yamada, K. Yano, Q. Xu and S. Fukuzumi, *J. Phys. Chem. C*, 2010, **114**, 16456-16462.
194 D. B. Grotjahn, D. B. Brown, J. K. Martin, D. C. Marelius, M.-C. Abadjian, H. N. Tran, G. Kalyuzhny, K. S. Vecchio, Z. G. Specht, S. A. Cortes-Llamas, V. Miranda-Soto, C. van Niekerk, C. E. Moore and A. L. Rheingold, *J. Am. Chem. Soc*., 2011, **133**, 19024-19027.
195 U. Hintermair, S. M. Hashmi, M. Elimelech and R. H. Crabtree, *J. Am. Chem. Soc*., 2012, **134**, 9785-9795.
196 K. R. Yang, A. J. Matula, G. Kwon, J. Hong, S. W. Sheehan, J. M. Thomsen, G. W. Brudvig, R. H. Crabtree, D. M. Tiede, L. X. Chen and V. S. Batista, *J. Am. Chem. Soc*., 2016, **138**, 5511-5514.
197 H. Junge, N. Marquet, A. Kammer, S. Denurra, M. Bauer, S. Wohlrab, F. Gärtner, M.-M. Pohl, A. Spannenberg, S. Gladiali and M. Beller, *Chem.–Eur. J.*, 2012, **18**, 12749-12758.
198 S. W. Sheehan, J. M. Thomsen, U. Hintermair, R. H. Crabtree, G. W. Brudvig and C. A. Schmuttenmaer, *Nat. Commun*., 2015, **6**, 6469.
199 A. Bucci, S. Dunn, G. Bellachioma, G. M. Rodriguez, C. Zuccaccia, C. Nervi and A. Macchioni, *ACS Catal*., 2017, **7**, 7788-7796.
200 G. M. Rodriguez, A. Bucci, R. Hutchinson, G. Bellachioma, C. Zuccaccia, S. Giovagnoli, H. Idriss and A. Macchioni, *ACS Energy Lett*., 2017, **2**, 105-110.
201 A. Petronilho, A. Llobet and M. Albrecht, *Inorg. Chem*., 2014, **53**, 12896-12901.
202 D. G. H. Hetterscheid, C. J. M. van der Ham, O. Diaz-Morales, M. W. G. M. (Tiny) Verhoeven, A. Longo, D. Banerjee, J. W. (Hans) Niemantsverdriet, J. N. H. Reekd and M. C. Feiters, *Phys. Chem. Chem. Phys*., 2016, **18**, 10931-10940.
203 Y. Isaka, S. Kato, D. Hong, T. Suenobu, Y. Yamada and S. Fukuzumi, J. *Mater. Chem. A*, 2015, **3**, 12404-12412.
204 I. Corbucci, K. Ellingwood, L. Fagiolari, C. Zuccaccia, F. Elisei, P. L. Gentili and A. Macchioni, *Catal. Today*, 2017, **290**, 10-18.
205 M. W. Kanan and D. G. Nocera, *Science*, 2008, **321**, 1072-1075.
206 Y. Surendranath, M. W. Kanan and D. G. Nocera, *J. Am. Chem. Soc*., 2010, **132**, 16501-16509.
207 M. W. Kanan, J. Yano, Y. Surendranath, M. Dincà, V. K. Yachandra and D. G. Nocera, *J. Am. Chem. Soc*., 2010, **132**, 13692-13701.
208 Y. Surendranath, D. A. Lutterman, Y. Liu and D. G. Nocera, *J. Am. Chem. Soc*., 2012, **134**, 6326-6336.
209 Q. Yin, J. M. Tan, C. Besson, Y. V. Geletii, D. G. Musaev, A. E. Kuznetsov, Z. Luo, K. I. Hardcastle and C. L. Hill, *Science*, 2010, **328**, 342-345.
210 N. D. Morris and T. E. Mallouk, *J. Am. Chem. Soc*., 2002, **124**, 11114-11121.
211 L. Eberson, *Electron Transfer Reactions in Organic Chemistr*y, Springer-Verlag, Berlin, 1987.
212 Z. Huang, Z. Luo, Y. V. Geletii, J. W. Vickers, Q. Yin, D. Wu, Y. Hou, Y. Ding, J. Song, D. G. Musaev, C. L. Hill and T. Lian, *J. Am. Chem. Soc*., 2011, **133**, 2068-2071.
213 F. Song, Y. Ding, B. Ma, C. Wang, Q. Wang, X. Du, S. Fua and J. Song, *Energy Environ. Sci*., **2013**, *6*, 1170-1184.
214 J. J. Stracke and R. G. Finke, *J. Am. Chem. Soc*., 2011, **133**, 14872-14875.
215 S. J. Folkman, J. Soriano-Lopez, J. R. Galán-Mascarós and R. G. Finke, *J. Am. Chem. Soc*., 2018, **140**, 12040-12055.
216 Y. Zhang, Y. Wang, X. Meng, L. Yu, Y. Ding, M. Chen, *J. Photochem. Photobiol. A: Chem*., 2018, **355**, 371–376

217 J. Soriano-López, D. G. Musaev, C. L. Hill, J. R. Galán-Mascarós, J. J. Carbó and J. M. Poblet, *J. Catal.*, 2017, **350**, 56-63.
218 S. Goberna-Ferró, L. Vigara, J. Soriano-López and J. R. Galán-Mascarós, *Inorg. Chem.*, 2012, **51**, 11707-11715.
219 M. Blasco-Ahicart, J. Soriano-López, J. J. Carbó, J. M. Poblet and J. R. Galan-Mascaros, *Nat. Chem*., 2018, **10**, 24-30.
220 D. Hong, J. Jung, J. Park, Y. Yamada, T. Suenobu, Y.-M. Lee, W. Nam and S. Fukuzumi, *Energy Environ. Sci*., 2012, **5**, 7606- 7616.
221 D. Shevchenko, M. F. Anderlund, A. Thapper and S. Styring, *Energy Environ. Sci.*, 2011, **4**, 1284-1287.
222 S. Fukuzumi, Y.-M. Lee and W. Nam, *Chem.–Eur. J*., 2018, **24**, 5016-5031.
223 S. Kato, J. Jung, T. Suenobu and S. Fukuzumi, *Energy Environ. Sci.*, 2013, **6**, 3756-3764.
224 J. W. Han, J. Jung, Y.-M. Lee, W. Nam and S. Fukuzumi, *Chem. Sci.*, 2017, **8**, 7119-7125.
225 H.-Y. Wang, E. Mijangos, S. Ott and A. Thapper, *Angew. Chem., Int. Ed*., 2014, **53**, 14499-14502.
226 T. Ishizuka, A. Watanabe, H. Kotani, D. Hong, K. Satonaka, T. Wada, Y. Shiota, K. Yoshizawa, K. Ohara, K. Yamaguchi, S. Kato, Shunichi Fukuzumi and T. Kojima, *Inorg. Chem*., 2016, **55**, 1154-1164.
227 J.-W. Wang, P. Sahoo and T.-B. Lu, *ACS Catal*., 2016, **6**, 5062-5068.
228 H.-Y. Du, S.-C. Chen, X.-J. Su, L. Jiao and M.-T. Zhang, *J. Am. Chem. Soc*., 2018, **140**, 1557-1565.
229 D. Das, S. Pattanayak, K. K. Singh, B. Garai and S. Sen Gupta, *Chem. Commun*., 2016, **52**, 11787-11790.
230 T. J. Collins, R. D. Powell, C. Slebodnick and E. S. Uffel, *J. Am. Chem. Soc*., 1991, **113**, 8419-8425.
231 S. Hong, F. F. Pfaff, E. Kwon, Y. Wang, M.-S. Seo, E. Bill, K. Ray and W. Nam, *Angew. Chem., Int. Ed*., 2014, **53**, 10403-10407; *Angew. Chem., Int. Ed*., 2017, **56**, 10613.
232 C. Saracini, D. D. Malik, M. Sankaralingam, Y.-M. Lee, W. Nam and S. Fukuzumi, *Inorg. Chem*., 2018, **57**, 10945-10952.
233 T. Nakazono, A. R. Parent and K. Sakai, *Chem. Commun*., 2013, **49**, 6325-6327.
234 T. Nakazono, A. R. Parent and K. Sakai, *Chem.–Eur. J*., 2015, **21**, 6723-6726.
235 D. Wang and J. T. Groves, *Proc. Natl. Acad. Sci. U.S.A*., 2013, **110**, 15579-15584.
236 A. Han, H. Jia, H. Ma, S. Ye, H. Wu, H. Lei, Y. Han, R. Cao, P. Du, P. *Phys. Chem. Chem. Phys*., 2014, **16**, 11224-11232.
237 W. Sinha, A. Mizrahi, A. Mahammed, B. Tumanskii and Z. Gross, *Inorg. Chem*., 2018, **57**, 478-485.
238 L. Xu, H. Lei, Z. Zhang, Z. Yao, J. Li, Z. Yu and R. Cao, *Phys. Chem. Chem. Phys*., 2017, **19**, 9755-9761.
239 Q. Daniel, R. B. Ambre, B. Zhang, B. Philippe, H. Chen, F. Li, K. Fan, S. Ahmadi, H. Rensmo and L. Sun, *ACS Catal*., 2017, **7**, 1143-1149.
240 M. D. Kärkäs, O. Verho, E. V. Johnston and B. Åkermark, B. *Chem. Rev*., 2014, **114**, 11863-12001.
241 G. C. Dismukes, R. Brimblecombe, G. A. N. Felton, R. S. Pryadun, J. E. Sheats, L. Spiccia and G. F. Swiegers, *Acc. Chem. Res.*, 2009, **42**, 1935-1943.
242 M. M. Najafpour, G. Renger, M. Hołyńska, A. N. Moghaddam, E.-M. Aro, R. Carpentier, H. Nishihara, J. J. Eaton-Rye, Jian-Ren Shen and S. Allakhverdiev, *Chem. Rev*., 2016, **116**, 2886-2936.
243 S. Paul, F. Neese and D. A. Pantazis, *Green Chem*., 2017, **19**, 2309-2325.
244 A. Izgorodin, R. Hocking, O. Winther-Jensen, M. Hilder, B. Winther-Jensen and D. R. MacFarlane, *Catal. Today*, 2013, **200**, 36-40.
245 C.-C. Yang, T. M. Eggenhuisen, M. Wolters, A. Agiral, H. Frei, P. E. de Jongh, K. P. de Jong and G. Mul, *ChemCatChem*, 2013, **5**, 550-556.
246 M. Yagi and K. Narita, *J. Am. Chem. Soc.*, 2004, **126**, 8084-8085.
247 K. Beckmann, H. Uchtenhagen, G. Berggren, M. F. Anderlund, A. Thapper, J. Messinger, S. Styring and P. Kurz, *Energy Environ. Sci.*, 2008, **1**, 668-676.
248 M. Mahdi Najafpour and A. N. Moghaddam, *Dalton Trans*., 2012, **41**, 10292-10297.
249 A. Singh, R. K. Hocking, S. L.-Y. Chang, B. M. George, M. Fehr, K. Lips, A. Schnegg and L. Spiccia, *Chem. Mater*., 2013, **25**, 1098-1108.
250 Y. Mousazade, M. R. Mohammadi, P. Chernev, R. Bikas, R. Bagheri, Z. Song, T. Lis, H. Dau and M. M. Najafpour, *Catal. Sci. Technol*., 2018, **8**, 4390-4398.
251 E. A. Mohamed, Z. N. Zahran and Y. Naruta, *J. Catal*., 2017, **352**, 293-299.
252 M. Guo, Y.-M. Lee, R. Gupta, M. S. Seo, T. Ohta, H.-H. Wang, H.-Y. Liu, S. N. Dhuri, R. Sarangi, S. Fukuzumi and W. Nam, *J. Am. Chem. Soc*., 2017, **139**, 15858-15867.
253 Y. Gao, T. Åkermark, J. Liu, L. Sun and B. Åkermark, *J. Am. Chem. Soc*., 2009, **131**, 8726-8727.
254 S. Kim, H. Park, M. S. Seo, M. Kubo, T. Ogura, J. Klajn, D. T. Gryko, J. S. Valentine and W. Nam, *J. Am. Chem. Soc*., 2010, **132**, 14030–14032.
255 R.-Z. Liao, M. D. Kärkäs, B.-L. Lee, B. Åkermark and P. E. M. Siegbahn, *Inorg. Chem*., 2015, **54**, 342-351.
256 R.-Z. Liao and P. E. M. Siegbahn, *ChemSusChem*, 2017, **10**, 4236-4263.
257 J.-W. Wang, W.-J. Liu, D.-C. Zhong and T.-B. Lu, *Coord. Chem. Rev*. 2019, **378**, 237-261.
258 J.-W. Wang, X.-Q. Zhang, H.-H. Huang and T.-B. Lu, *ChemCatChem*, 2016, **8**, 3287-3293.
259 J. Shen, M. Wang, T. He, J. Jiang and M. Hu, *Chem. Commun*., 2018, **54**, 9019-9022.
260 M. M. Najafpour and H. Feizi, *Dalton Trans*., 2018, **47**, 6519-652.
261 H. Feizi, F. Shiri, R. Bagheri, J. P. Singh, K. H. Chae, Z. Song and M. M. Najafpour, *Catal. Sci. Technol*., 2018, **8**, 3954-3968.
262 C. J. M. van der Hama, F. I Ş ı k, T. W. G. M. Verhoeven, J. W. (Hans) Niemantsverdriet, D. G. H. Hetterscheid, *Catal. Tod*ay, 2017, **290**, 33-38.
263 L. Yu, J. Lin, M. Zheng, M. Chen and Y. Ding, *Chem. Commun*., 2018, **54**, 354-357.
264 S. M. Barnett, K. I. Goldberg and J. M. Mayer, *Nat. Chem*., 2012, **4**, 498-502.
265 X. Jiang, J. Li, B. Yang, X.-Z. Wei, B.-W. Dong, Y. Kao, M.-Y. Huang, C.-H. Tung and L.-Z. Wu, *Angew. Chem., Int. Ed*., 2018, **57**, 7850-7854.

266 F. Chen, N. Wang, H. Lei, D. Guo, H. Liu, Z. Zhang, W. Zhang, W. Lai and R. Cao, *Inorg. Chem*., 2017, **56**, 13368-13375.
267 P. Garrido-Barros, I. Funes-Ardoiz, S. Drouet, J. Benet-Buchholz, F. Maseras and A. Llobet, *J. Am. Chem. Soc*., 2015, **137**, 6758-6761.
268 X. J. Su, M. Gao, L. Jiao, R. Z. Liao, P. E. M. Siegbahn, J. P. Cheng and M. T. Zhang, M. T. *Angew. Chem., Int. Ed*., 2015, **54**, 4909-4914.
269 R.-J. Xiang, H.-Y. Wang, Z.-J. ; Xin, C.-B. Li, Y.-X. Lu, X.-W. Gao, H.-M. Sun and R. Cao, *Chem.–Eur. J*., 2016, **22**, 1602-1607.
270 P. Garrido-Barros, C. Gimbert-Surinach, D. Moonshiram, A. Picon, P. Monge, V. S. Batista and A. Llobet, *J. Am. Chem. Soc*., 2017, **139**, 12907-12910.
271 S. J. Koepke, K. M. Light, P. E. VanNatta, K. M. Wiley and M. T. Kieber-Emmons. *J. Am. Chem. So*c., 2017, **139**, 8586-8600.
272 I. Gamba, Z. Codola, J. Lloret-Fillol and M. Costas, *Coord. Chem. Rev*., 2017, **334**, 2-24.
273 M. M. Najafpour and S. M. Hosseini, *Int. J. Hydrogen Energy*, 2016, **41**, 22635-22642.
274 M. M. Najafpour, R. Safdari, F. Ebrahimi, P. Rafighi and R. Bagheri, *Dalton Trans*., 2016, **45**, 2618-2623.
275 Z. Codola, M. Costas, J. Lloret-Fillol L. Gomez, S. T. Kleespies and L. Que, Jr., *Nat. Commun*., 2015, **6**, 5865.
276 M. M. Najafpour, A. N. Moghaddam, D. J. Sedigh and M. Holynska, *Catal. Sci. Technol*., 2014, **4**, 30-33.
277 A. J. Jasniewski and L. Que, Jr., *Chem. Rev*., 2018, **118**, 2554-2592.
278 T. J. Collins and A. D. Ryabov, *Chem. Rev*., 2017, **117**, 9140-9162.
279 G. Olivo, O. Cusso, M. Borrell and M. Costas, *J. Biol. Inorg. Chem*., 2017, **22**, 425-452.
280 G. Olivo, O. Cusso and M. Costas, *Chem.–Aisan J*., 2016, **11**, 3148-3158.
281 A. Fuerstner, *ACS Cent. Sci*., 2016, 2, 778-789.
282 S. Sahu and D. P. Goldberg, *J. Am. Chem. Soc*., 2016, **138**, 11410-11428.
283 X.-H. Yang, R.-J. Song, Y.-X. Xie and J.-H. Li, *ChemCatChem*, 2016, **8**, 2429-2445.
284 J. L. Fillol, Z. Codola, I. Garcia-Bosch, L. Gomez, J. J. Pla and M. Costas, *Nat. Chem*., 2011, **3**, 807-813.
285 D. Hong, S. Mandal, Y. Yamada, Y.-M. Lee, W. Nam, A. Llobet and S. Fukuzumi, *Inorg. Chem*., 2013, **52**, 9522-9531.
286 G. Chen, L. Chen, S.-M. Ng, W.-L. Man and T.-C. Lau, *Angew. Chem., Int. Ed*., 2013, **52**, 1789-1791.
287 C. Panda, J. Debgupta, D. D. Díaz, K. K. Singh, S. Sen Gupta and B. B. Dhar, *J. Am. Chem. Soc*., 2014, **136**, 12273-12282.
288 M. Zheng, Y. Ding, X. Cao, T. Tian and J. Lin, *Appl. Catal. B: Environ*., 2018, **237**, 1091-1100.
289 A. Lewandowska-Andralojc and D. E. Polyansky, *J. Phys. Chem. A*, 2013, **117**, 10311-1031.
290 M. Ghosh, K. K. Singh, C. Panda, A. Weitz, M. P. Hendrich, T. J. Collins, B. B. Dhar and S. Sen Gupta, *J. Am. Chem. Soc*., 2014, **136**, 9524−9527.
291 W. C. Ellis, N. D. McDaniel, S. Bernhard and T. J. Collins, *J. Am. Chem. Soc*., 2010, **132**, 10990-10991.
292 S. Pattanayak, D. R. Chowdhury, B. Garai, K. K. Singh, A. Paul, B. B. Dhar and S. Sen Gupta, *Chem.–Eur. J*., 2017, **23**, 3414-3424.
293 G. Warner, M. Mills, C. Enslin, S. Pattanayak, C. Panda, T. Panda, S. Sen Gupta, A. D. Ryabov and T. J. Collins, *Chem.–Eur. J*., 2015, **21**, 6226-6233.
294 M. Okamura, M. Kondo, R. Kuga, Y. Kurashige, T. Yanai, S. Hayami, V. K. K. Praneeth, M. Yoshida, K. Yoneda, S. Kawata and S. Masaoka, *Nature*, 2016, **530**, 465-468.
295 M. Xie, X. Xiong, L. Yang, X. Shi, A. M. Asiri and X. Sun, *Chem. Commun*., 2018, **54**, 2300-2303.
296 J. S. Kanady, E. Y. Tsui, M. W. Day and T. Agapie, *Science*, 2011, **333**, 733-736.
297 S. Fukuzumi, Y. Morimoto, H. Kotani, P. Naumov, Y.-M. Lee and W. Nam, *Nat. Chem.,* 2010, **2**, 756-759.
298 E. Y. Tsui, R. Tran, J. Yano and T. Agapie, *Nat. Chem.*, 2013, **5**, 293-299.
299 J. Chen, Y.-M. Lee, K. M. Davis, X. Wu, M. S. Seo, K.-B. Cho, H. Yoon, Y. J. Park, S. Fukuzumi, Y. N. Pushkar, W. Nam, *J. Am. Chem. Soc.,* 2013, **135**, 6388-6391.
300 S. Bang, Y.-M. Lee, S. Hong, Y. Nishida, M. S. Seo, R. Sarangi, S. Fukuzumi and W. Nam, *Nat. Chem*., 2014, **6**, 934-940.
301 V. Krewald, F. Neese and D. A. Pantazis, *Phys. Chem. Chem. Phys*., 2016, **18**, 10739-10750.
302 D. A. Pantazis, *ACS Catal*., 2018, **8**, 9477-9507
303 Y. Yamada, K. Yano, D. Hong and S. Fukuzumi, *Phys. Chem. Chem. Phys*., 2012, **14**, 5753-5760.
304 D. Hong, Y. Yamada, T. Nagatomi, Y. Takai and S. Fukuzumi, *J. Am. Chem. Soc*., 2012, **134**, 19572-19575.
305 Z. Wu, Z. Zou, J. Huang and F. Gao, *ACS Appl. Mater. Interfaces*, 2018, **10**, 26283-26292.
306 L. He, B. Cui, B. Hu, J. Liu, K. Tian, M. Wang, Y. Song, S. Fang, Z. Zhang and Q. Jia, *ACS Appl. Energy Mater*., 2018, **1**, 3915-3928.
307 Md. S. Islam, M. Kim, Xiaoyan Jin, S. M. Oh, N.-S. Lee, H. Kim and S.-J. Hwang, *ACS Energy Lett*., 2018, **3**, 952-960.
308 Y. Liu, Q. Li, R. Si, G.-D. Li, W. Li, D.-P. Liu, D. Wang, L. Sun, Y. Zhang and X. Zou, *Adv. Mater*., 2017, **29**, 1606200.
309 B. Zhang, H. Wang, Z. Zuo, H. Wang and J. Zhang, *J. Mater. Chem. A*, 2018, **6**, 15728-15737.
310 Z. Ma, Q. Zhao, J. Li, B. Tang, Z. Zhang and X. Wang, *Electrochim. Acta*, 2018, **260**, 82-91.
311 M. Qian, S. Cui, D. Jiang, L. Zhang and P. Du, *Adv. Mater*., 2017, **29**, 1704075.
312 P. Li, X. Duan, Y. Kuang, Y. Li, G. Zhang, W. Liu and X. Sun, *Adv. Energy Mater*., 2018, **8**, 1703341.
313 D. Zhou, Z. Cai, Y. Jia, X. Xiong, Q. Xie, S. Wang, Y. Zhang, W. Liu, H. Duan and X. Sun, *Nanoscale Horiz*., 2018, **3**, 532-537.
314 X. Xu, F. Song and X. Hu, *Nat. Commun*., 2016, **7**, 12324.
315 H. Zhou, F. Yu, Q. Zhu, J. Sun, F. Qin, L. Yu, J. Bao, Y. Yu, S. Chen and Z. Ren, *Energy Environ. Sci*., 2018, **11**, 2858-2864.
316 Y. Yamada, K. Oyama, T. Suenobu and S. Fukuzumi, *Chem. Commun*., 2017, **53**, 3418-3421.
317 B. Dong, X. Zhao, G.-Q. Han, X. Li, X. Shang, Y.-R. Liu, W.-H. Hu, Y.-M. Chai, H. Zhao and C.-G. Liu, *J. Mater. Chem. A*, 2016, **4**, 13499–13508.

TOC

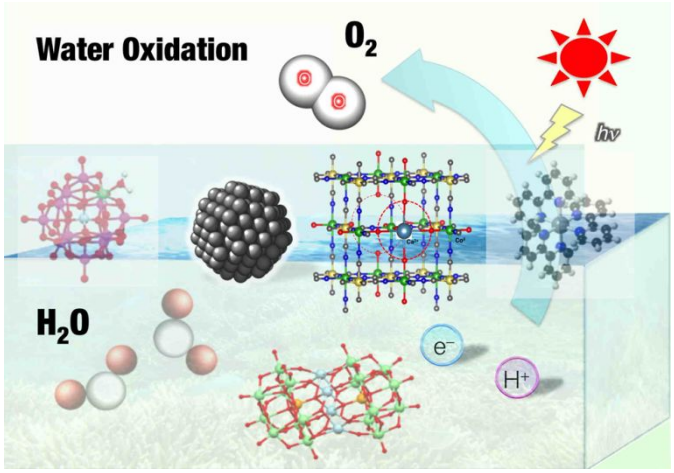

Text for TOC

This review discusses kinetics and mechanisms of chemical, electrocatalytic and photocatalytic water oxidation by homogeneous and heterogeneous transition metal catalysts.